LA-UR- 98-4876

Approved for public release; distribution is unlimited.

Title: The Use of Propagation Path Corrections to Improve Seismic Event Location in Western China

RECEIVED
APR 0 6 1998
OSTI

Author(s): Allen H. Cogbill, EES-3
Lee K. Steck, EES-3

Submitted to: DOE/NN-20

MASTER

DISTRIBUTION OF THIS DOCUMENT IS UNLIMITED

19980423 170

DTIC QUALITY INSPECTED 4

Los Alamos
NATIONAL LABORATORY

Los Alamos National Laboratory, an affirmative action/equal opportunity employer, is operated by the University of California for the U.S. Department of Energy under contract W-7405-ENG-36. By acceptance of this article, the publisher recognizes that the U.S. Government retains a nonexclusive, royalty-free license to publish or reproduce the published form of this contribution, or to allow others to do so, for U.S. Government purposes. Los Alamos National Laboratory requests that the publisher identify this article as work performed under the auspices of the U.S. Department of Energy. Los Alamos National Laboratory strongly supports academic freedom and a researcher's right to publish; as an institution, however, the Laboratory does not endorse the viewpoint of a publication or guarantee its technical correctness.

Form No. 836 R6
ST 2629 8/96

DISCLAIMER

This report was prepared as an account of work sponsored by an agency of the United States Government. Neither the United States Government nor any agency thereof, nor any of their employees, makes any warranty, express or implied, or assumes any legal liability or responsibility for the accuracy, completeness, or usefulness of any information, apparatus, product, or process disclosed, or represents that its use would not infringe privately owned rights. Reference herein to any specific commercial product, process, or service by trade name, trademark, manufacturer, or otherwise does not necessarily constitute or imply its endorsement, recommendation, or favoring by the United States Government or any agency thereof. The views and opinions of authors expressed herein do not necessarily state or reflect those of the United States Government or any agency thereof.

Abstract

In an effort to improve our ability to locate events in western China using only regional data, we have developed propagation path corrections to seismic travel times, and applied such corrections using both traditional location routines as well as a nonlinear grid search method. Thus far, we have concentrated on corrections to observed P arrival times. We have constructed such corrections by using travel time observations available from the USGS Earthquake Data Reports, as well as data reported by the ISC. We have also constructed corrections for six stations that are a part of the International Monitoring System. For each station having sufficient data, we produce a map of the travel-time residuals from all located events. Large-amplitude residuals are removed by median filtering, and the resulting data are gridded. For a given source location, the correction at a particular station is then interpolated from the correction grid associated with the station. We have constrained the magnitude of the corrections to be ≤ 3 s. We have evaluated the utility of the calculated corrections by applying the corrections to the regional relocation of 10 well-located Chinese nuclear tests, as well as a single, well-located aftershock in nearby Kyrgyzstan.

The use of corrections having magnitudes > 2 s is troubling when using traditional location codes, as the corrections amount to a nonlinear perturbation correction, and when large may destabilize the location algorithm. Partly for this reason, we have begun using grid search methods to relocate regional events. Such methods are easy to implement and fully nonlinear. Moreover, the misfit function used to locate the event can very easily be changed; we have used L_1- and L_2-norm misfit functions, for example. Instances in which multiple local minima occur in a location problem are easily recognized by simply contouring or otherwise displaying the misfit function. Although grid search methods are not nearly as computationally efficient as more traditional methods, their use in regional locations problems, where the number of observations is small, seems well-warranted, as a much better idea of the uncertainty of the location can be gained.

Introduction

This report is a progress report focusing on efforts we have made to improve the performance of the regional location of seismic events in western China and the surrounding regions. The impetus of the study is, of course, the Comprehensive Test Ban Treaty (CTBT), which, if ratified, would essentially ban all nuclear testing by the treaty's signatories. Our focus is on regional location, rather than teleseismic location, because of our interest in locating rather small seismic events. We believe that large explosive events will be easily detected and rather well-located, and are therefore of less interest than the multitude of small ($m_b < 4$) seismic events that occur both naturally and as the result of mining detonations or explosive testing (not necessarily nuclear).

We recognize that, in the absence of depth phases such as pP, the depth of a seismic event detected using a regional network of stations is very poorly constrained, except for the few cases where an event may occur extremely close to a station. Our efforts thus far have *not* concentrated on the estimation of the depth of a seismic event, despite the fact that a well-constrained depth can be a good discriminant between a naturally-occuring seismic event and an explosion. Rather, we have endeavored to more accurately estimate the epicenter of regionally-detected events; the estimation of the depth of such events has been deferred. Additionally, we have begun to use nonlinear location methods, largely in the hope that such methods can provide better estimates of the uncertainty associated with an event's location.

Our major product thus far is a suite of corrections that may be used to improve the location of seismic events in the study area. To date, we have developed such corrections and applied them to the relocation of events for which we have very good estimates of their actual locations. We have been able to demonstrate that the corrections that we have developed improve the location of events, at least in those few areas where events having known locations are available.

Known Event Locations (aka Ground Truth)

A major stumbling block in the effort to develop better location methods has been the scarcity of relatively recent (i.e., recent enough to have been digitally recorded) known event locations in China. Chinese earthquake catalogs are not readily available in the West. We have not been able to identify any published information that would provide accurate event locations for seismic events that would have been well-recorded regionally. However, from Gupta (1995) we have good estimates of some of the locations of the Chinese nuclear events detonated at the Chinese test site near Lop Nor. Inasmuch as the Chinese test site is of obvious interest from the viewpoint of the CTBT, such locations provide us a badly-needed set of unclassified data that can be used to evaluate the corrections that we have developed. Additionally, we have a very well-determined location of a regionally-recorded aftershock of the Kyrgyzstan earthquake of 19 August 1992 (Ghose and others, 1997), which is quite close to the Chinese border.

The locations of the events that are described above are known well enough that such events can be used to ascertain whether a calculated location is close to an actual location. Another issue is what type of events should be used to construct corrections; that is, how well should the locations of the events used to construct corrections be known? This is an important issue that is discussed in greater detail in the next section.

Development of Corrections

Our general philosophy in our efforts to improve event location has been to develop propagation path corrections, rather than trying to develop three-dimensional velocity models. There are two reasons for this approach. First, the location codes in use at both the prototype International Data Center (IDC) and the U. S. National Data Center use the interpolation of standard travel time curves as the primary method for calculating travel times from an event to a station. We believe that, unless one has a very dense network of stations and events, it is difficult to develop a three-dimensional velocity model that is close enough to reality to properly correct such travel time curves on a regional basis. However, it is straightforward to try to develop corrections (primarily travel-time, but azimuthal and slowness corrections, as well) to the travel-time curves, if one has a sufficient number of reasonably well-located events. The drawback to such an approach is that a relatively high level of seismicity is required in order to garner enough data to form good statistics. Much of China and the surrounding areas have a relatively high level of seismicity, with some notable exceptions. Second, the construction of corrections in this manner is imminently suited to the use of calibration events. While we have no calibration events thus far, should any be used, the measurements from such events could be readily incorporated into our corrections.

The propagation path corrections that we develop are source-to-station corrections. Thus, each station has its own set of corrections; the corrections vary spatially. In principle, the corrections should vary as a function of source depth, as well. However, because we are most interested in surface sources, we have restricted our investigations to such sources, and therefore the corrections we develop are not necessarily applicable to deeper sources.

The events that we have used to construct corrections have been seismic events located in our region of interest that meet a certain event criteria. Specifically, the criteria that we have used is that (1) the depth of the event must be ≤ 33 km, (2) the maximum azimuthal gap between locating stations used to locate an event is $\leq 180°$, and (3) the maximum observed travel-time

residual used to construct corrections is ≤ 3 s in modulus. We present evidence later to justify our use of these parameters.

Seismicity of China

Seismicity maps derived from the United States Geological Survey's National Earthquake Information Center (NEIC) Earthquake Data Report (USGS EDR) for years 1990 through 1995 and the International Seismological Centre (ISC) Catalog for years 1986-1993 are shown in Figures 1-2. The locations of stations reporting to each of these catalogs are shown in their respective maps. A seismicity map from the Reviewed Event Bulletin (REB) of the prototype International Monitoring System (IMS) for years 1995 through 1996, showing both reporting as well as proposed station locations, is given in Figure 3. Frequency-magnitude plots, Figure 4, indicate that the NEIC and ISC catalogs are incomplete below about magnitude 4 or 5. The IDC catalog is similarly incomplete.

Travel Time Data

Most of the results we report here are based upon data published either by the NEIC or by the International Seismological Centre (ISC). Both these organizations gather phase data (primarily travel-time data) and locate seismic events using the compiled phase data. Each organization accepts travel-time data from a large number of seismological observatories. We denote stations that report to the NEIC as NEIC stations, whereas those reporting to the ISC we term ISC stations. There is considerable overlap; many observatories report to both organizations. Of course, the stations of greatest interest to the CTBT are the IMS primary stations. However, few of these have been established in the vicinity of China, and effectively none was operating during the time period 1990-1992, the period for which we have reliable locations for some of the Chinese nuclear events. However, using the NEIC and ISC station data permits us to (a) develop propagation path corrections and evaluate the utility of such corrections and (b) still provides useful information, for some of the NEIC/ISC stations (*e.g.*, **LZH**) are slated to become IMS stations, and several of the NEIC/ISC stations are to become auxiliary IMS stations.

Although both the NEIC and the ISC use the Jeffreys-Bullen (J-B) travel-time tables for locating events, NEIC's location procedure is somewhat different from the ISC's. A major difference is that the NEIC location procedure is to locate an event, then discard observations whose travel-time residuals exceed 3 standard deviations in magnitude, then relocate the event. The ISC does not discard observations. The NEIC procedure rejects spurious observations and seems to provide for a more reliable solution that that of the ISC.

In addition to the NEIC and ISC data sets, we have also used the travel time residuals reported by the IDC (in the form of the REB) for the time period January 1995 through September 1997. The shorter time interval results in fewer data being available, especially because some of the IDC stations were not established at the beginning of the time period, but came on-line later. Still, sufficient data are available to permit a preliminary analysis of six IMS stations.

Variances of the Travel Times

Variances for the travel times reported in both the NEIC and the ISC reports differ widely, depending upon the station. For a given station, however, the data reported by the ISC and the NEIC seems to have about the same statistics. Figures 5-6 are histograms of the reported travel-time residuals at stations **LZH** and **BJI**, respectively. Only residuals < 6 s in modulus were used to create the figures. When the range of residuals is restricted to this interval, the variances of the two data sets are approximately the same for all of the 49 stations

that we have used in this study. This fact permits us to combine the data from the NEIC (1994 through 1995) and ISC (1986 through 1993) catalogs into a single data set prior to developing propagation path corrections.

Travel time data reported in the IDC's REB appear to have smaller variances than the data found in the NEIC and ISC catalogs. Figures 7-9 are histograms of the travel time data from all six of the IMS stations (**BJT, HIA, NIL, PDY, ULN,** and **ZAL**) that we have used in this study. With the single exception of **ZAL**, these station show very few travel-time residuals > 2 s in magnitude.

Propagation Path Corrections

The IDC uses the IASPEI 1991 (*iasp91*) earth velocity model for locating seismic events, whereas both the NEIC and the ISC use the J-B model. In order to use a consistent set of event data, we relocated all of the NEIC and ISC data using the LocSAT location algorithm and the *ak135* velocity model, which differs from *iasp91* only in its treatment of certain core phases. At regional distances, the travel times of both the *iasp91* and the *ak135* models are identical. The travel time residuals from these relocated events were used to develop propagation path corrections. When relocating events, we used only those phases used for location by the NEIC or the ISC. However, all residuals from all phases in the data sets were retained for later analysis. Because of the method that NEIC used to discard observations, this means that some of the residuals that go into the analysis data set might be rather large. However, the fact that we restrict our analysis to residuals ≤ 3 s in magnitude eliminates concerns about large residuals.

We have constructed propagation path corrections for travel times by mapping observed travel time residuals at a given station as a function of position. The maps that we have constructed are relatively smooth, which provides some confidence that the maps are not merely maps of observation error, but represent underlying velocity variations.

We constructed the propagation path correction maps as follows. For the NEIC and ISC stations, we combined all the NEIC (1994-1995) and ISC (1986-1993) observations into a single data set, then for each station, tabulated all the travel-time residuals from regional events (specifically, events occurring between latitude 20°-55°N., longitude 65°-115°E.) Then, only those residuals meeting our selection criteria (max azimuthal gap ≤ 180°, depth ≤ 33 km, residuals ≤ 3 s in magnitude) were used. Then the residuals for a particular station were interpolated (gridded) using a minimum curvature spline under tension (Smith & Wessell, 1990), with a grid increment of 15′ of arc. The tension parameters used were 0.6 for interior nodes and 0.8 for boundary nodes.

The algorithm used constrains a grid point by a data value when a data value lies within the grid pixel. In order to insure that only a single data value was present per grid square, a block median filter was run over the data set prior to interpolation. The 15′ discretization size was used for the block median operation, as well. Thus, if more than one event occured within a 15′ by 15′ region, the median value of the residuals for those events was used to constrain the value at that grid node. Propagation path correction surfaces for 49 NEIC/ISC stations and 6 IMS stations were constructed using this method. The surfaces for the 6 IMS stations are shown as Figures 10-15. Typically, the amount of data used to construct the corresponding surfaces for the NEIC and ISC stations was greater than that used for the IMS stations, most of which have been online for < 2 years. The data distributions shown for IMS stations **NIL** and **ZAL**

are representative of the data density available for the NEIC and ISC stations.

The correction surfaces can be used to correct the travel-times calculated from either the *iasp91* or the *ak135* velocity model. In other words, the travel time from a point in the study region to a particular station is calculated by calculating the time from the earth velocity model, correcting for elevation and ellipticity effects, and then adding the time interpolated from the correction surface. Due to the method of surface construction, the calculated correction will always be ≤ 3 s in magnitude. Because the station correction calculated in this manner depends upon the location of the source, we term the corrections *source-specific station corrections*, or *SSSCs*, after Bratt & Bache (1988).

Some limitations of the SSSC should be pointed out. First, these are only applicable to shallow events, as we have restricted to ≤ 33 km the depth range of the travel time data used to construct the corrections. Second, our imposition of a ±3 second limitation to the travel-time data is rather arbitrary. It certainly rejects travel-time outliers, but it limits the magnitude of the calculated corrections, as well. It is possible that the SSSCs should be larger in some areas. However, at the moment we are only able to evaluate the effectiveness of the SSSCs at two locations; we simply do not have sufficient ground truth available to permit us to address how to restrict the range of travel-time residuals used to construct the corrections.

Regional Location of Events

Within China, the spacing of stations reporting to western data centers is typically well under 1000 km, except in the northeast, the southeast, and in the interior of western China. Western China is of particular interest to this report, as it is the location of the Chinese nuclear test site near Lop Nor. In the region around Lop Nor, station spacing approaches 2000 km. Because of the relative lack of very well-located natural earthquakes in this region, and because of Lop Nor's importance to the CTBT, we have chosen to look in detail at the locations of nuclear tests at Lop Nor. This topic has been addressed in part by Gupta (1995), who describes a Joint Epicenter Determination (JED) of Lop Nor nuclear explosions. The JED method can provide accurate locations of a set of nearby seismic events relative to one event of the set (the "master event") (Douglas, 1967). If the location of the master event is accurately known, then all events will be well-located. To accurately locate his master events, Gupta (1995) analyzed several types of commercial satellite imagery.

In our study, we re-analyze ten Lop Nor explosions in the context of regional seismic event location, using only the 10 closest stations. For four of these explosions, Gupta's (1995) JED locations are available for use as ground truth. The average error vector of these four JED locations from the ISC location was 5.32 km. For nuclear tests occuring after Gupta's 1995 study, we compare our "regional" relocations (see below) to catalog locations derived from arrival times recorded at hundreds of stations.

Arrival time data in our analysis were taken from the USGS EDRs. Only first-arriving P-wave data were used. By sequentially removing the more distant of the 10 stations one at a time and relocating the explosions, we can evaluate the usefulness of the LocSAT method. Figure 16 summarizes the hypocentral error vector of the relocations *versus* maximum azimuthal gap and number of stations used, for each of the ten nuclear events analyzed. In these locations, we used the *ak135* velocity model, with ellipticity and elevation corrections applied. No propagation path corrections were applied. When depths are constrained to 0 in the solution, the regional relocations are quite good, even when as few as

3 stations are used. However, when depths are unconstrained, location errors are distinctly larger (Figure 17). The location performance of the depth-constrained solutions led us to the maximum azimuthal gap criterion of $\leq 180°$; events having azimuthal gaps exceeding 180° appear to have a large chance of being significantly mislocated. If a more conservative criterion of $< 90°$ were used instead, the number of events used to construct the correction surfaces would be far fewer; it is not yet clear whether the reliability of the locations used after applying such a criterion would be substantially better.

When SSSCs are employed, there is an overall reduction in mislocation errors and locations tend to become more stabilized (compare Figures 16&18 and 17&19). Figures 20-29 shows map views of mislocation for each of the analyzed nuclear shots at Lop Nor, as the number of stations used in the location is reduced from 10 to 4 (or 3, if depth is constrained). Black and red symbols indicate locations for which SSSCs were used (free depth and depth fixed at 0, respectively), while green and blue symbols indicate the absence of SSSCs in the location (free depth and depth fixed at 0, respectively). Also provided in each panel of the figures is a map of the locations of the reporting EDR stations closest to the Lop Nor test site, in a window from 20°-60° latitude and from 65°-115° longitude.

We also relocated, using only regional observations, an aftershock of the 1992 Suusamyr, Kyrgyzstan, earthquake. Several hundred aftershocks of this earthquake were very well-located in a special study by Ghose and others (1997); however, only one of these hundreds of events was listed in the EDRs. Figure 30 summarizes the relocation accuracy achieved; Figure 31 shows the station distribution used for the event, as well as a mislocation plot.

The relatively high accuracy of the regional locations, even in relatively poor network geometries, is encouraging. However, there is no reason to believe that other regions in China would behave as well as the two we have studied. Clearly, additional events having well-determined locations are needed to evaluate regional location bias.

Hypocenter Locations Using Grid Search Methods

Standard linearized hypocenter location methods, such as that used by LocSAT, suffer from several limitations. Typical problems include the potential to become trapped in local minima and the trade-off between origin-time and depth. To remedy these shortcomings, we have begun developing a non-linear, global, grid-search hypocenter location algorithm (Sambridge & Kennett, 1986; Kennett, 1992). The advantages of this approach are: 1) it is a global minimization method, 2) the error volume at any given misfit level is provided, 3) the origin-time minimization is independent of the spatial coordinates, and 4) any desired norm may be used to calculate the misfit function, enabling the use of unusual error distribution functions (*e.g.*, Jeffreys, 1932). In our implementation, we create a dense grid of points in the volume surrounding the suspected hypocenter. Traveltimes for all desired phases are calculated from each point on the grid to all stations, and these travel times may be corrected for Earth's ellipticity, station elevation, and for propagation path effects. For every (x,y,z) location on the grid, the best-fit origin time is found by finding the minimum misfit between the observed traveltime data and the calculated traveltimes for a set of gridded origin times around the input origin time. The origin time with the smallest misfit for that (x,y,z) location is kept. We have applied this algorithm to the nuclear explosion data from Lop Nor, where we have some measure of ground truth, and compare its results to the LocSAT algorithm.

Table 1. Comparison of the location performance of LocSAT versus the gridding algorithm used here. Errors shown are in equivalent radial kilometers, using 10 stations and 4 stations for comparison. Where LocSAT did not converge to a solution, the "DIV" is shown. Depths were constrained to 0, and propagation path corrections were used.

	10 Stations		4 Stations	
Event	LocSAT	GRID	LocSAT	GRID
Aug90	2.27	3.70	9.63	5.73
Aug95	3.54	7.87	3.30	7.87
Jul96	4.89	9.66	26.34	15.71
Jun94	6.92	4.63	6.78	4.63
Jun96	0.86	2.32	DIV	2.77
May90	9.99	16.66	7.03	7.19
May92	2.44	5.73	DIV	18.98
Oct93	7.54	8.89	7.25	5.73
Oct94	12.04	18.57	DIV	6.94
Sep92	11.68	5.72	12.62	31.74

For the examples given below, we perform our grid search over a 1° by 1° by 50 km grid volume surrounding the best-known location (either from satellite or teleseismic methods as outlined previously). The horizontal grid spacing used is 1.6 km (1′ of arc), while the vertical spacing is 10 km. Traveltime misfits are calculated with the L_1 norm in this example.

In terms of the accuracy of epicentral solution, LocSAT's performance seems somewhat better than the grid algorithm when 10 stations are used. When only 4 stations are used, though, the results are inconclusive. The fact that an L_1 norm was used for the grid solutions, whereas LocSAT uses an L_2 norm, may contribute to the observed differences in location accuracy. Of course, the grid method always provides a solution, whereas the LocSAT method occasionally diverges.

Use of the gridding method permits one to more easily visualize the shape of the uncertainty volume associated with a hypocentral solution. At each grid node in the volume searched, a value of the misfit function is calculated. The calculated misfit function can therefore be displayed rather easily, which can lead to some useful information. For example consider the calculated location of the August 1990 Chinese event (Table 1). LocSAT calculates an error ellipse associated with the solution number and geometry of the stations used in the solution. Figure 32 shows its error ellipse, together with contours of the misfit function calculated using the grid search method (at depth = 0). The misfit function shown in the figure plainly shows that two minima are present, information that is lacking in the (linearized) LocSAT results. Figure 33 shows the volume of the misfit function for selected constant values of the function.

Our use of the grid methods is in its infancy and is presented here largely to indicate the directions our research is taking. Due to its relative computational inefficiency, the grid search method is unlikely to be a competitor for more traditional location schemes such as LocSAT. However, it can provide improved information about the uncertainties in a solution; any such additional information is likely to be welcome in special event studies.

Conclusions

We have attacked the problem of improving regional epicentral event locations by developing propagation path corrections for individual stations in western China and the surrounding regions. The corrections that we have developed are defined on a geographic grid, thus enabling them to be used easily as part of a travel-time calculation. We have been able to evaluate the efficacy of such corrections in only two locations. One such location is the Chinese nuclear test site near Lop Nor, where 10 seismic events having well-known locations are available. The other location is in Kyrgyzstan, not far from the Chinese border, where a single aftershock (out of several hundred recorded) from a detailed after-

shock study has been used to evaluate the utility of the propagation path corrections. We conclude that the use of propagation path corrections usually improves location accuracy and, moreover, seems to improve the convergence of the LocSAT location algorithm, which falls into a class of commonly-used location codes.

Additionally, we have begun an investigation of the use of grid search algorithms for location. Such algorithms are completely non-linear and always provide a solution, provided that the event location is within the area of the grid search. Such grid search algorithms have a number of advantages over conventional location algorithms. In particular, the use of such algorithms can provide one with a much better idea of the (random) uncertainty of the event location. Although such algorithms are substantially slower to execute than a conventional location code, in regional location problems of high interest, the added information available from the use of the grid search approach makes the use of such an algorithm highly desirable.

References Cited

Billings, Stephen D., 1994, Simulated annealing for earthquake location, *Geophys. Jour. International*, **118**, 680-694.

Bratt, Steven R. and Thomas C. Bache, 1988, Locating events with a sparse network of regional arrays, *Bull. Seis. Soc. Am.*, **78**(2), 780-798.

Douglas, A., 1967, Joint epicenter determination, *Nature*, **215**, 47-48.

Jeffreys, Harold, 1932, An alternative to the rejection of observations, *Proceeding of the Royal Society of London*, **137A**, 78-87.

Ghose, S., R. J. Mellors, A. M. Korjenkov, M. W. Hamburger, T. L. Pavlis, G. L. Pavlis, M. Omuraliev, E. Mamyrov, and A. R. Muraliev, 1997, The M_s = 7.3 1992 Suusamyr, Kyrgyzstan, earthquake in the Tien Shan: 2. Aftershock focal mechanisms and surface deformation, *Bull. Seis. Soc. Am.*, **87**(1), 23-38.

Gupta, Vipin, 1995, Locating nuclear explosions at the Chinese test site near Lop Nor, *Science and Global Security*, **5**, 205-244.

Kennett, B.L.N., 1992, Locating oceanic earthquakes-the influence of regional models and location criteria, *Geophys. J. Int.*, **108**, 848-845.

Kennett, B. L. N and E. R. Engdahl, 1991, Traveltimes for global earthquake location and phase identification, *Geophysical Journal International*, **165**, 429-465.

Sambridge, Malcolm, and B. L. N. Kennett, 1986, A novel method of hypocentre location, *Geophys. Jour. Royal Astron. Soc.*, **87**, 679-697.

Smith, W. H. F. and P. Wessel, 1990, Gridding with continuous curvature splines under tension, *Geophysics*, **55**(3), 293-305.

Figure Captions

Figure 1. Seismicity map of western China and environs derived from the NEIC EDRs. Triangles are the locations of seismic stations reporting to the NEIC.

Figure 2. Seismicity map of western China and environs derived from the ISC earthquake catalog. Triangles are the locations of seismic stations reporting to the ISC.

Figure 3. Seismicity map of western China and environs derived from the Reviewed Event Bulletin of the prototype IDC. The locations (triangles) and station designations of the IMS stations are also shown.

Figure 4. Histogram of the magnitudes reported in the NEIC and the ISC earthquake catalogs.

Figure 5. Histograms of travel-time residuals measured from P arrivals at **LZH**, a station located in central China. Both residuals reported in the NEIC EDRs as well as the ISC catalog are shown.

Figure 6. Histograms of travel-time residuals measured from P arrivals at **BJI**, a station located in central China. Both residuals reported in the NEIC EDRs as well as the ISC catalog are shown.

Figure 7. Histogram of travel-time residuals from P arrivals measured at IMS stations **BJT** and **HIA**.

Figure 8. Histogram of travel-time residuals from P arrivals measured at IMS stations **NIL** and **PDY**.

Figure 9. Histogram of travel-time residuals from P arrivals measured at IMS stations **ULN** and **ZAL**

Figure 10. Travel-time correction surface calculated for IMS station **BJT**. The position of **BJT** is shown as a white triangle. Corrections shown on this map are added to the travel times conventionally calculated from a point on the map to the station location.

Figure 11. Travel-time correction surface calculated for IMS station **HIA**. The position of **HIA** is shown as a white triangle. Corrections shown on this map are added to the travel times conventionally calculated from a point on the map to the station location.

Figure 12. Travel-time correction surface calculated for IMS station **NIL**. The position of **NIL** is shown as a white triangle. Corrections shown on this map are added to the travel times conventionally calculated from a point on the map to the station location.

Figure 13. Travel-time correction surface calculated for IMS station **PDY**. The position of **PDY** is shown as a white triangle. Corrections shown on this map are added to the travel times conventionally calculated from a point on the map to the station location.

Figure 14. Travel-time correction surface calculated for IMS station **ULN**. The position of **ULN** is shown as a white triangle. Corrections shown on this map are added to the travel times conventionally calculated from a point on the map to the station location.

Figure 15. Travel-time correction surface calculated for IMS station **ZAL**. The position of **ZAL** is shown as a white triangle. Corrections shown on this map are added to the travel times conventionally calculated from a point on the map to the station location.

Figure 16. Summary of epicentral mislocations for regionally-located nuclear events conducted at the Chinese nuclear test site near Lop Nor. Depths have been constrained to 0 in the location process. The results corresponding to the relocations using 10,9, ... ,3 stations are shown.

Figure 17. Summary of epicentral mislocations for regionally-located nuclear events conducted at the Chinese nuclear test site near Lop Nor. Depths were unconstrained in the location process.. The results corresponding to the relocations using 10,9, ... ,4 stations are shown.

Figure 18. Summary of epicentral mislocations for regionally-located nuclear events conducted at the Chinese nuclear test site near Lop Nor. Source-specific station corrections were applied, and

depths were been constrained to 0 in the location process.. The results corresponding to the relocations using 10,9, ... ,3 stations are shown.

Figure 19. Summary of epicentral mislocations for regionally-located nuclear events conducted at the Chinese nuclear test site near Lop Nor. Source-specific station corrections were applied, but depths were unconstrained in the location process. The results corresponding to the relocations using 10,9, ... ,4 stations are shown.

Figure 20. Locations of the 10 closest stations reporting travel times from the May 1990 Chinese nuclear test at Lop Nor, along with a mislocation diagram that shows the location error as the number of stations used in the location calculation is decreased from 10,9, ..., 3. Black and red symbols indicate location calculations in which SSSCs were used (free depth and depth fixed at 0, respectively), while green and blue symbols idicate location calculation in which SSSCs were not used (free depth and depth fixed at 0, respectively). The purple star plotted at the origin in the mislocation diagram represents the actual location of the event.

Figure 21. Locations of the 10 closest stations reporting travel times from the August 1990 Chinese nuclear test at Lop Nor, along with a mislocation diagram that shows the location error as the number of stations used in the location calculation is decreased from 10,9, ..., 3. Black and red symbols indicate location calculations in which SSSCs were used (free depth and depth fixed at 0, respectively), while green and blue symbols idicate location calculation in which SSSCs were not used (free depth and depth fixed at 0, respectively). The purple star plotted at the origin in the mislocation diagram represents the actual location of the event.

Figure 22. Locations of the closest stations reporting travel times from the May 1992 Chinese nuclear test at Lop Nor, along with a mislocation diagram that shows the location error as the number of stations used in the location calculation is decreased from 10,9, ..., 3. Note the lack of many stations within in the aperture of the map; this is especially curious, for the May 1992 event was one of the largest of the Chinese underground nuclear tests, and was well-recorded throughout the world. Black and red symbols indicate location calculations in which SSSCs were used (free depth and depth fixed at 0, respectively), while green and blue symbols idicate location calculation in which SSSCs were not used (free depth and depth fixed at 0, respectively). The purple star plotted at the origin in the mislocation diagram represents the actual location of the event.

Figure 23. Locations of the 10 closest stations reporting travel times from the September 1992 Chinese nuclear test at Lop Nor, along with a mislocation diagram that shows the location error as the number of stations used in the location calculation is decreased from 10,9, ..., 3. Black and red symbols indicate location calculations in which SSSCs were used (free depth and depth fixed at 0, respectively), while green and blue symbols idicate location calculation in which SSSCs were not used (free depth and depth fixed at 0, respectively). The purple star plotted at the origin in the mislocation diagram represents the actual location of the event.

Figure 24. Locations of the 10 closest stations reporting travel times from the October 1993 Chinese nuclear test at Lop Nor, along with a mislocation diagram that shows the location error as the number of stations used in the location calculation is decreased from 10,9, ..., 3. Black and red symbols indicate location calculations in which SSSCs were used (free depth and depth fixed at 0, respectively), while green and blue symbols idicate location calculation in which SSSCs were not used (free depth and depth fixed at 0, respectively). The purple star plotted at the origin in the mislocation diagram represents the actual location of the event.

Figure 25. Locations of the 10 closest stations reporting travel times from the June 1994 Chinese nuclear test at Lop Nor, along with a mislocation diagram that shows the location error as the number of stations used in the location calculation is decreased from 10,9, ..., 3. Black and red symbols indicate location calculations in which SSSCs were used (free depth and depth fixed at 0, respectively), while green and blue symbols idicate location calculation in which SSSCs were not used (free depth and depth fixed at 0, respectively). The purple star plotted at the origin in the mislocation diagram represents the actual location of the event.

Figure 26. Locations of the 10 closest stations reporting travel times from the October 1994 Chinese

nuclear test at Lop Nor, along with a mislocation diagram that shows the location error as the number of stations used in the location calculation is decreased from 10,9, ..., 3. Black and red symbols indicate location calculations in which SSSCs were used (free depth and depth fixed at 0, respectively), while green and blue symbols idicate location calculation in which SSSCs were not used (free depth and depth fixed at 0, respectively). The purple star plotted at the origin in the mislocation diagram represents the actual location of the event.

Figure 27. Locations of the 10 closest stations reporting travel times from the August 1995 Chinese nuclear test at Lop Nor, along with a mislocation diagram that shows the location error as the number of stations used in the location calculation is decreased from 10,9, ..., 3. Black and red symbols indicate location calculations in which SSSCs were used (free depth and depth fixed at 0, respectively), while green and blue symbols idicate location calculation in which SSSCs were not used (free depth and depth fixed at 0, respectively). The purple star plotted at the origin in the mislocation diagram represents the actual location of the event.

Figure 28. Locations of the 10 closest stations reporting travel times from the June 1996 Chinese nuclear test at Lop Nor, along with a mislocation diagram that shows the location error as the number of stations used in the location calculation is decreased from 10,9, ..., 3. Black and red symbols indicate location calculations in which SSSCs were used (free depth and depth fixed at 0, respectively), while green and blue symbols idicate location calculation in which SSSCs were not used (free depth and depth fixed at 0, respectively). The purple star plotted at the origin in the mislocation diagram represents the actual location of the event.

Figure 29. Locations of the 10 closest stations reporting travel times from the July 1996 Chinese nuclear test at Lop Nor, along with a mislocation diagram that shows the location error as the number of stations used in the location calculation is decreased from 10,9, ..., 3. Black and red symbols indicate location calculations in which SSSCs were used (free depth and depth fixed at 0, respectively), while green and blue symbols idicate location calculation in which SSSCs were not used (free depth and depth fixed at 0, respectively). The purple star plotted at the origin in the mislocation diagram represents the actual location of the event.

Figure 30. Summary of epicentral mislocation for the regionally-located Kyrgyzstan aftershock event. Source-specific station corrections were applied, and the depth was constrained to 6.2 km (the depth determined by the special aftershock study) in the location process.

Figure 31. Locations of the 10 closest stations reporting travel times from the Kyrgyzstan aftershock event, along with a mislocation diagram that shows the location error as the number of stations used in the location calculation is decreased from 10,9, ..., 3. Black and red symbols indicate location calculations in which SSSCs were used (free depth and depth fixed at 0, respectively), while green and blue symbols idicate location calculation in which SSSCs were not used (free depth and depth fixed at 0, respectively).

Figure 32. Contours of the misfit function calculated by the grid search location algorithm for the August 1990 Chinese nuclear event. Only 4 stations were used for this relocation calculation. An L_1 norm was used to calculated the misfit function. For comparision, the confidence ellipse calculated by LocSAT is shown; the confidence ellipse is calculated using an assumed travel-time error of 2 s at all reporting stations.

Figure 33. Diagram showing the volume associated with the misfit function calculated by the grid search location algorithm for the August 1990 Chinese nuclear event. Only 4 stations were used for this relocation calculation. An L_1 norm was used to calculated the misfit function. The volume shown is the volume associated with a constant misfit value of 0.1, 2.0, and 7.3 s, respectively.

Chinese Seismicity from NEIC

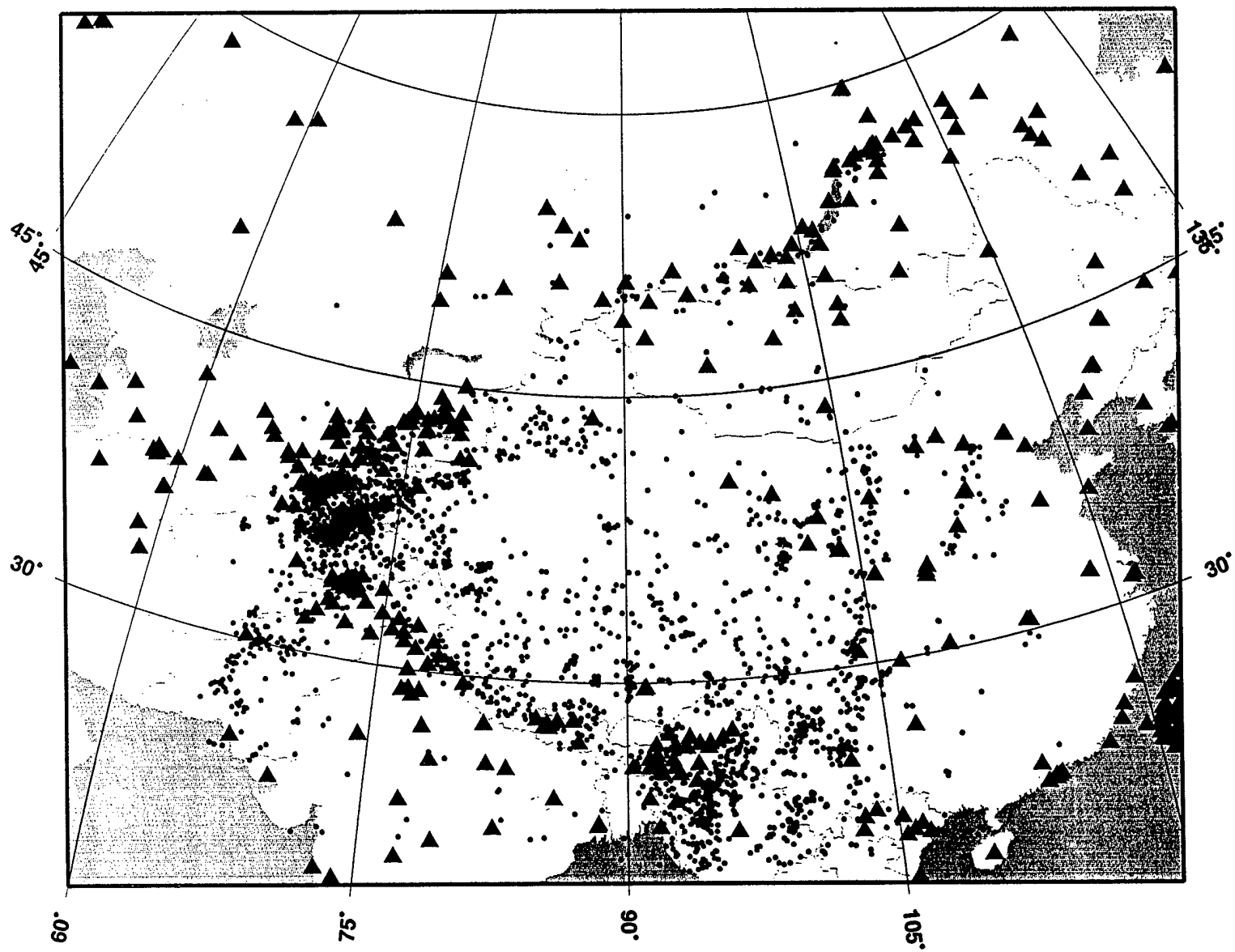

Figure 1

Chinese Seismicity from ISC

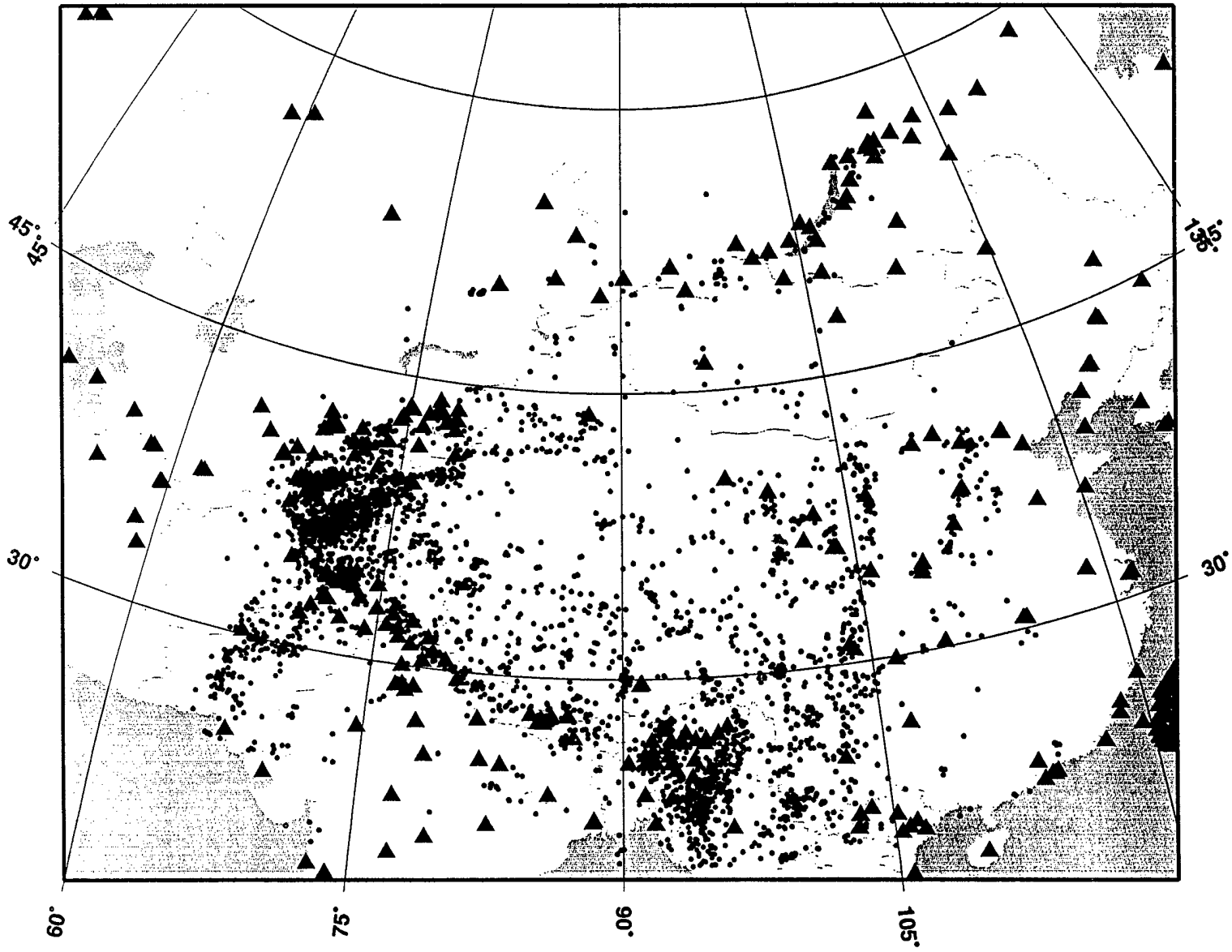

Figure 2.

Chinese Seismicity from PIDC

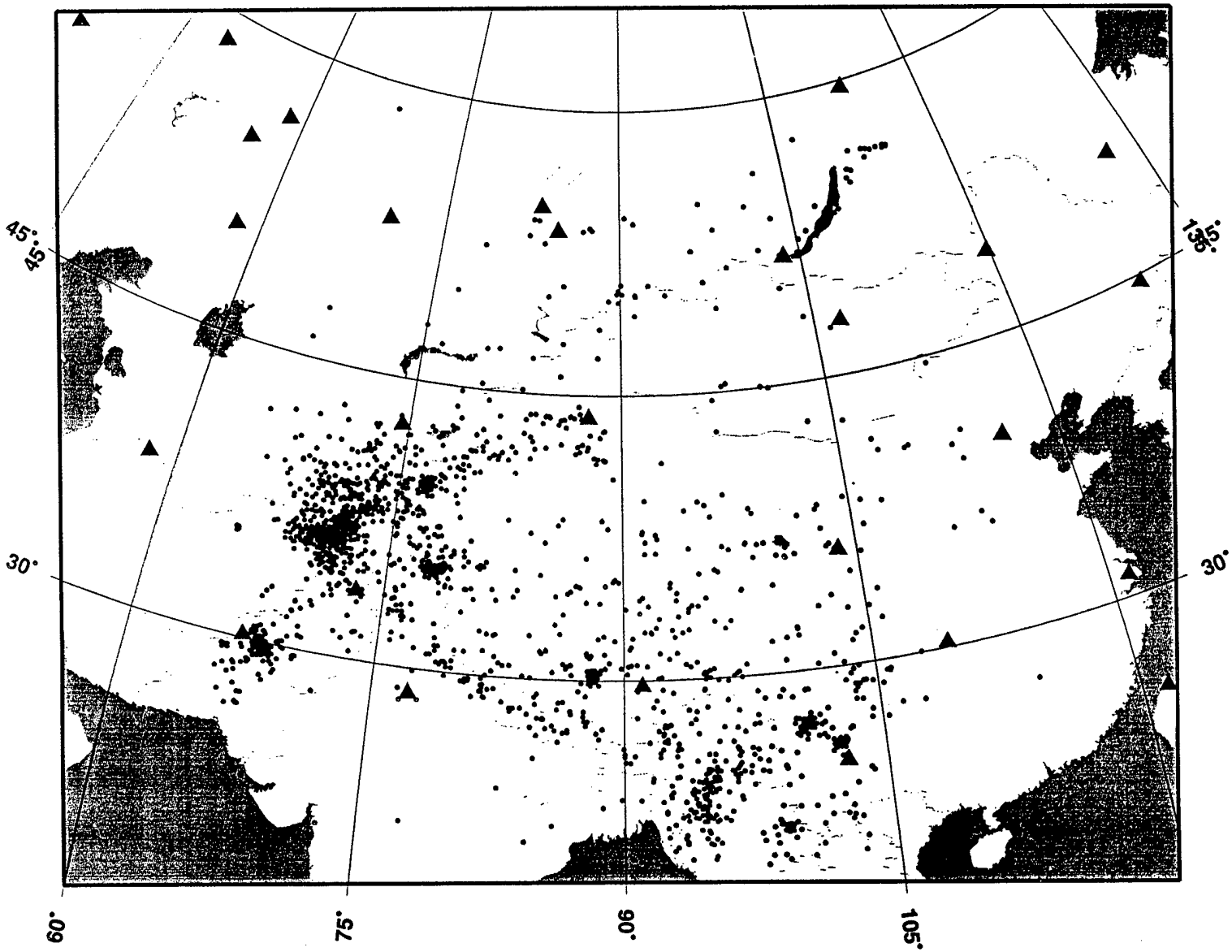

Figure 3.

Magnitude Distrbutions

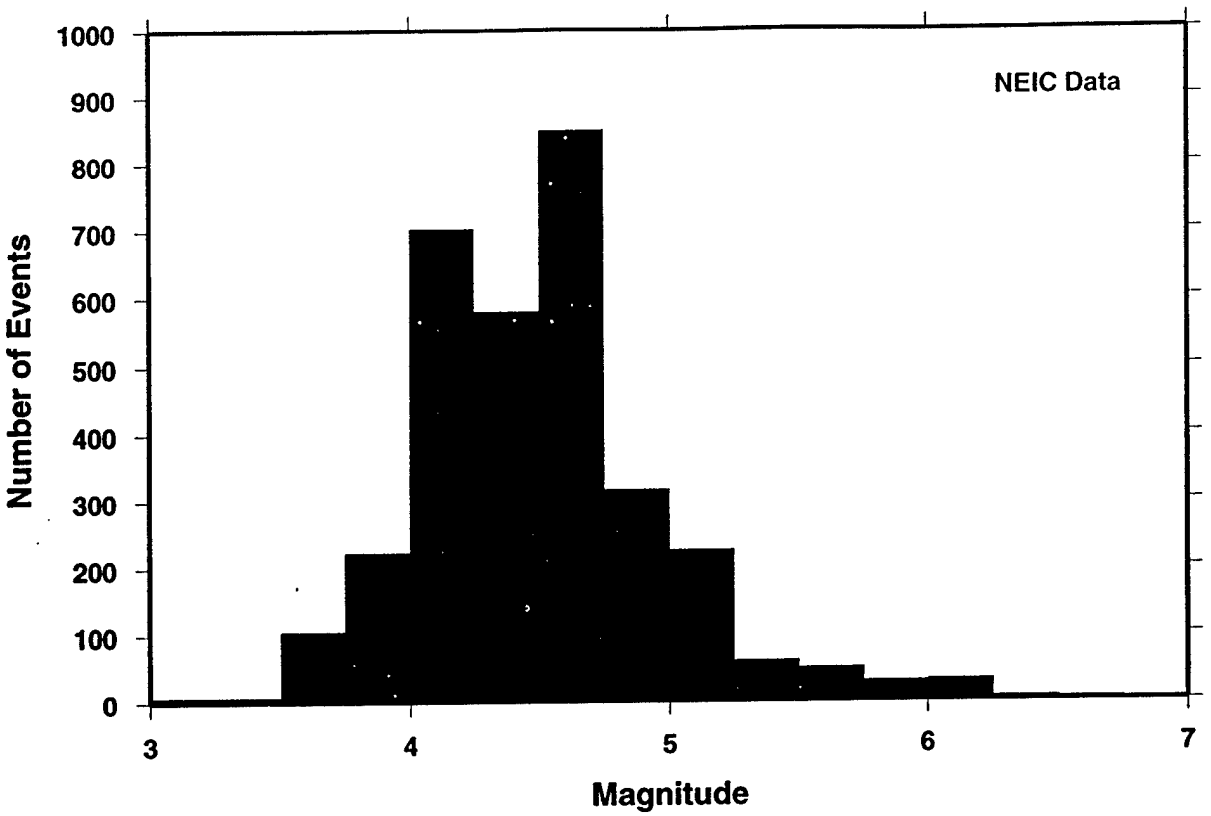

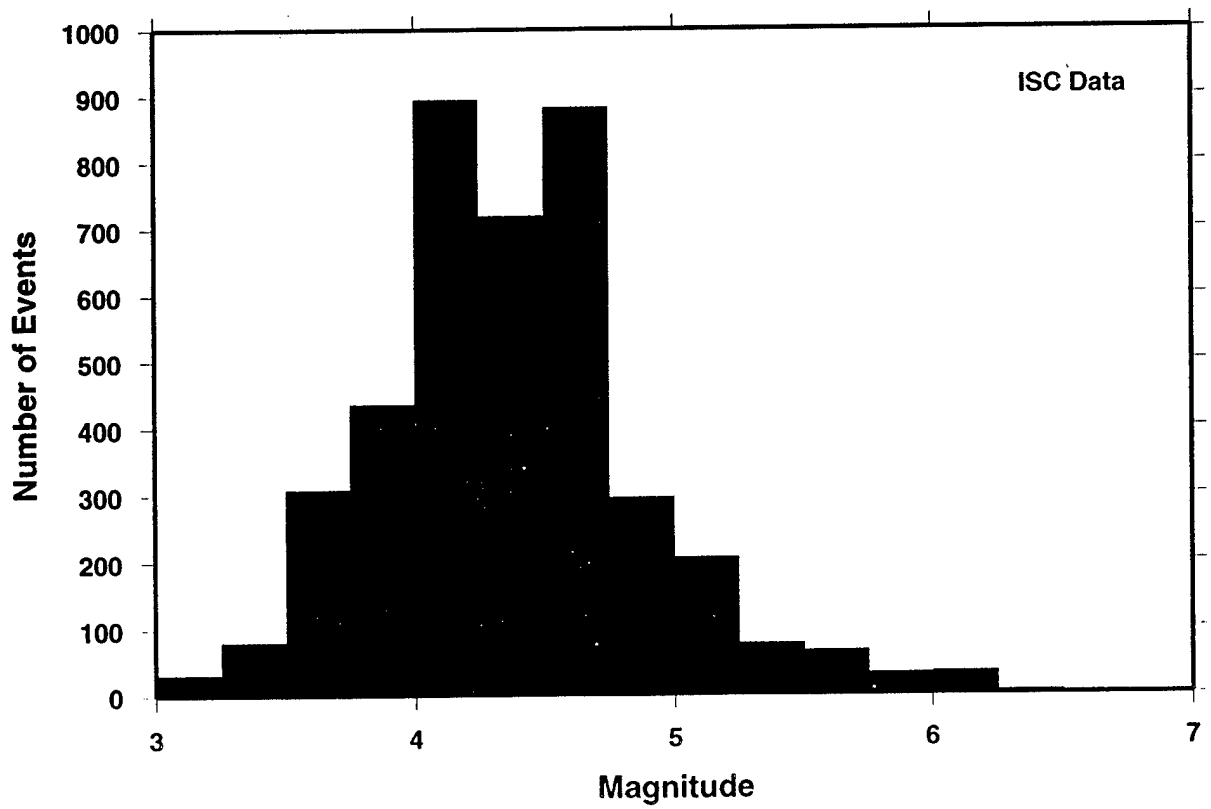

Figure 4.

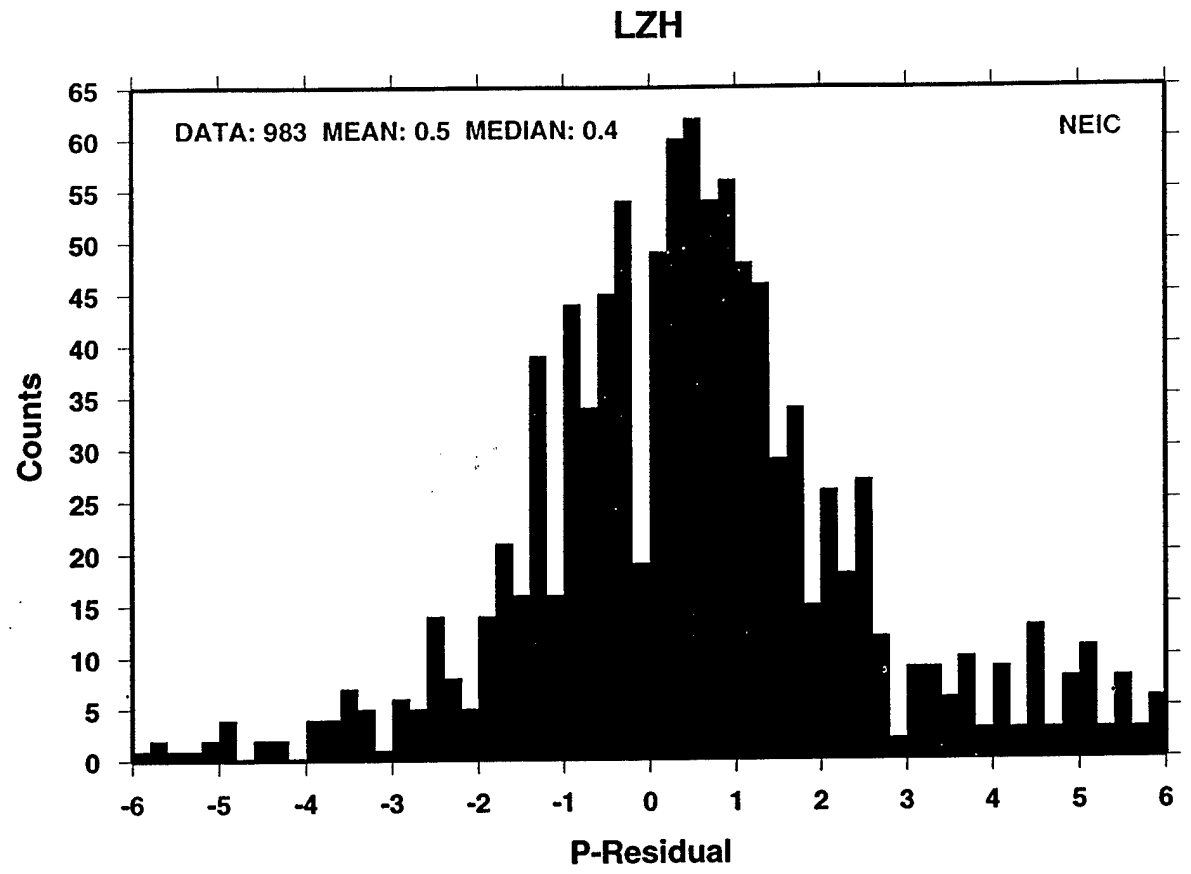
LZH
DATA: 983 MEAN: 0.5 MEDIAN: 0.4
NEIC
Counts
P-Residual
65
60
55
50
45
40
35
30
25
20
15
10
5
0
-6
-5
-4
-3
-2
-1
0
1
2
3
4
5
6

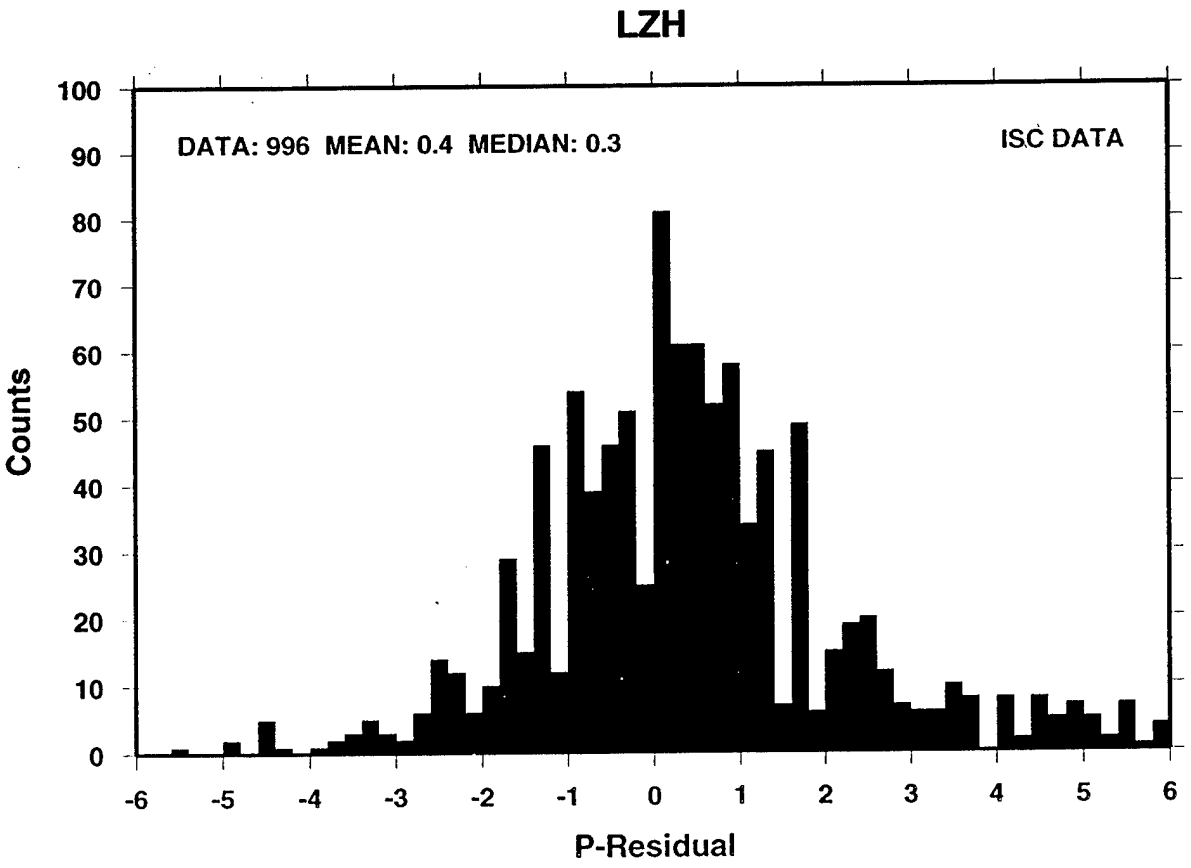
LZH
DATA: 996 MEAN: 0.4 MEDIAN: 0.3
ISC DATA
Counts
P-Residual
100
90
80
70
60
50
40
30
20
10
0
-6
-5
-4
-3
-2
-1
0
1
2
3
4
5
6

Figure 5.

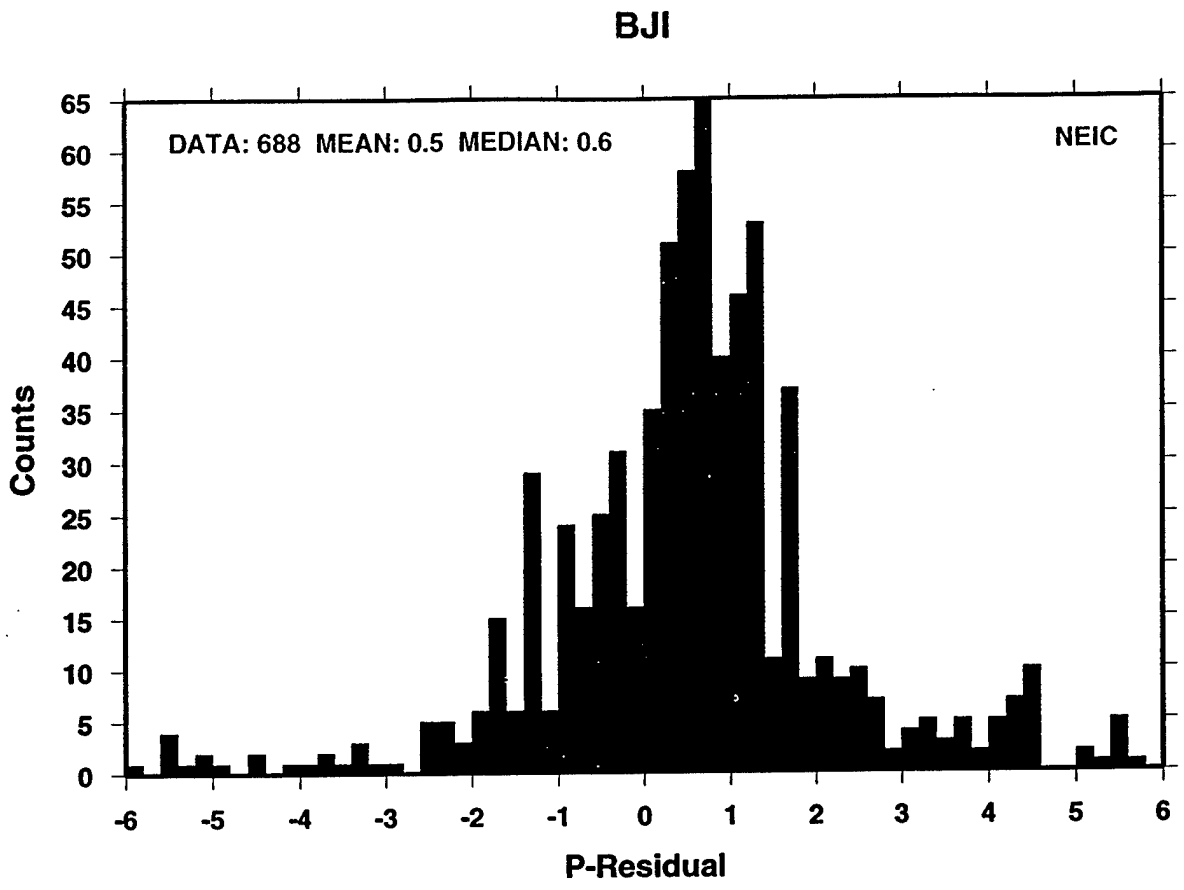
BJI
DATA: 688 MEAN: 0.5 MEDIAN: 0.6
NEIC
Counts
P-Residual
0
5
10
15
20
25
30
35
40
45
50
55
60
65
-6
-5
-4
-3
-2
-1
0
1
2
3
4
5
6

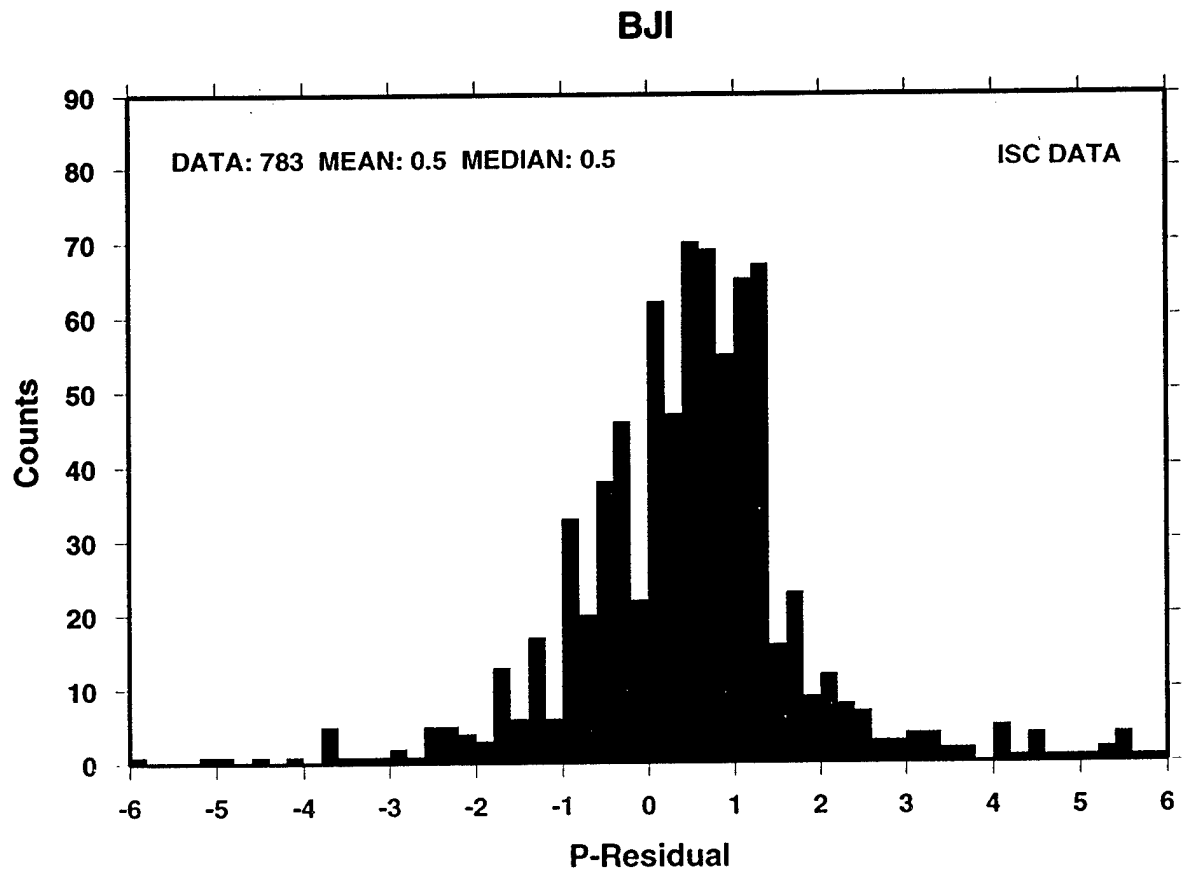
BJI
DATA: 783 MEAN: 0.5 MEDIAN: 0.5
ISC DATA
Counts
P-Residual
0
10
20
30
40
50
60
70
80
90
-6
-5
-4
-3
-2
-1
0
1
2
3
4
5
6

Figure 6.

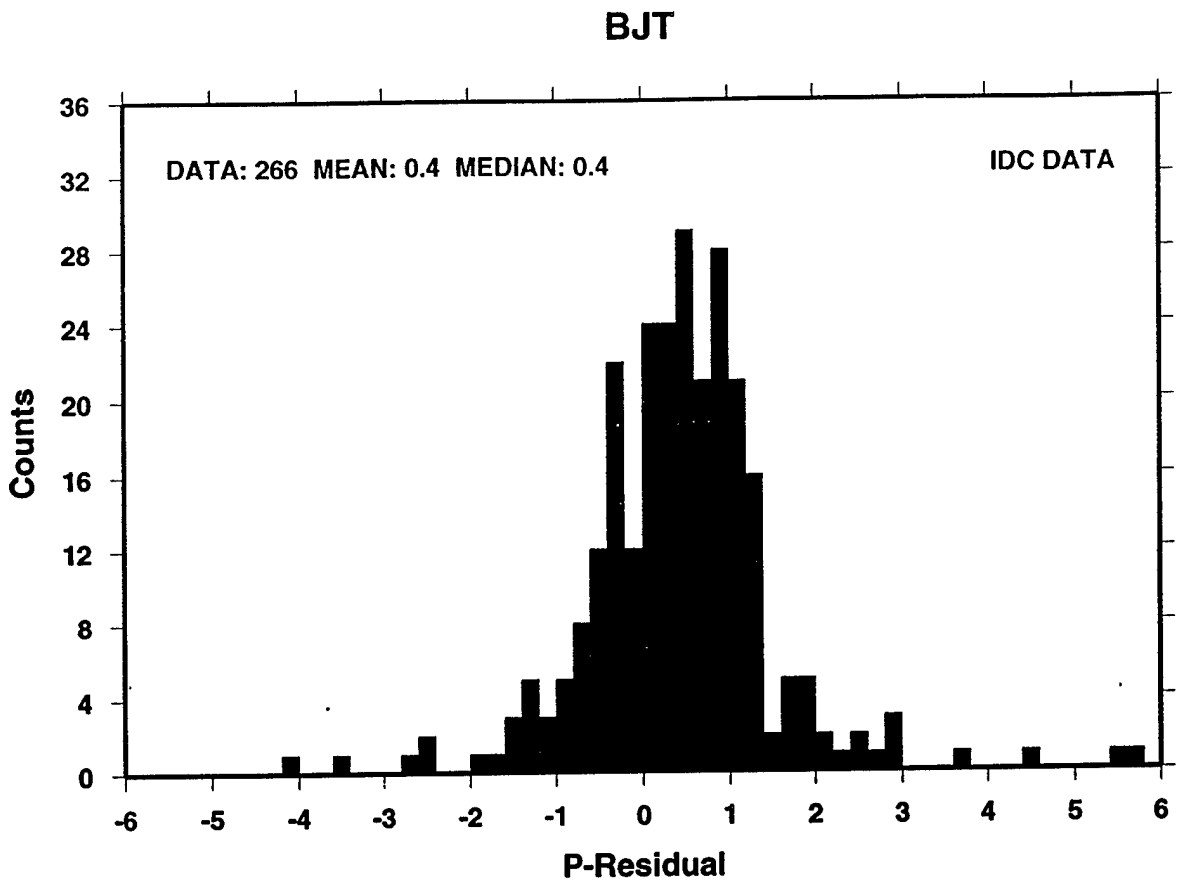
BJT
DATA: 266 MEAN: 0.4 MEDIAN: 0.4
IDC DATA
Counts
P-Residual
0
4
8
12
16
20
24
28
32
36
-6
-5
-4
-3
-2
-1
0
1
2
3
4
5
6

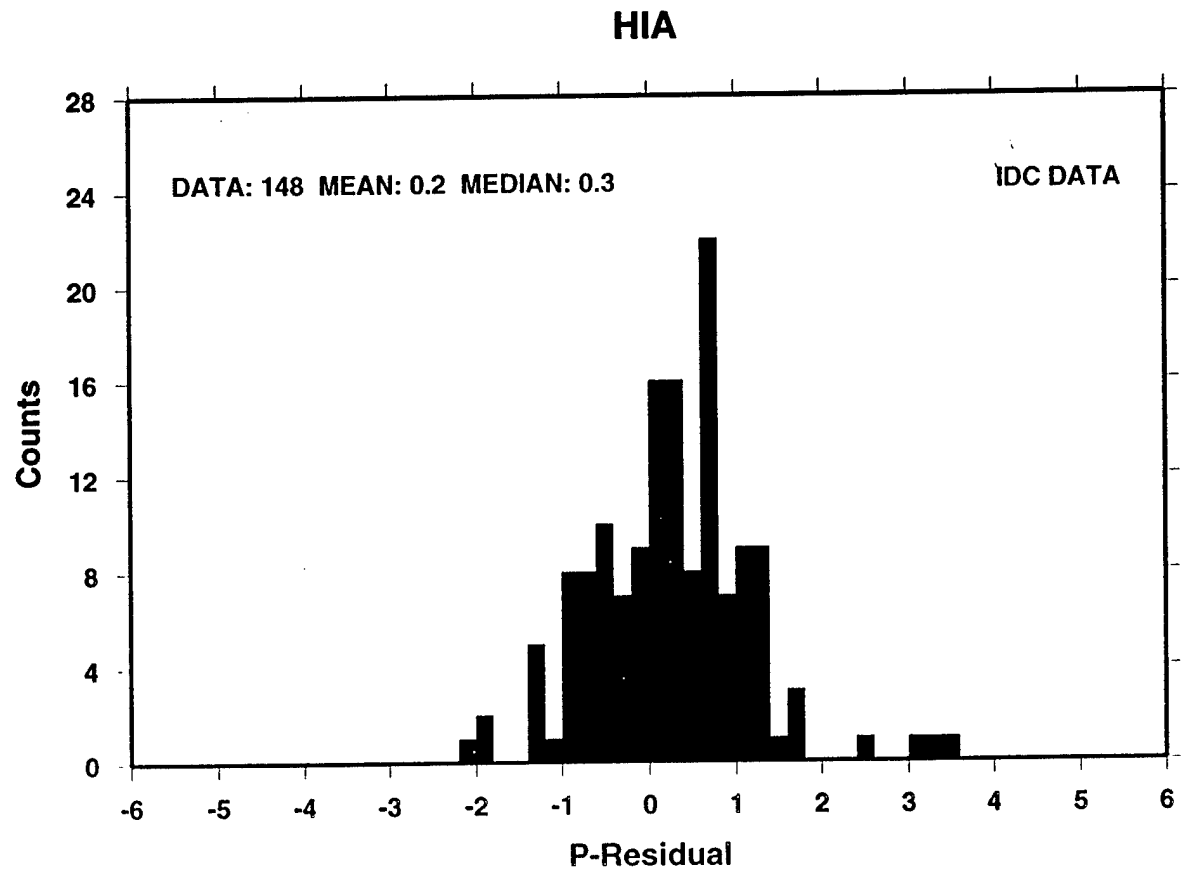
HIA
DATA: 148 MEAN: 0.2 MEDIAN: 0.3
IDC DATA
Counts
P-Residual
0
4
8
12
16
20
24
28
-6
-5
-4
-3
-2
-1
0
1
2
3
4
5
6

Figure 7.

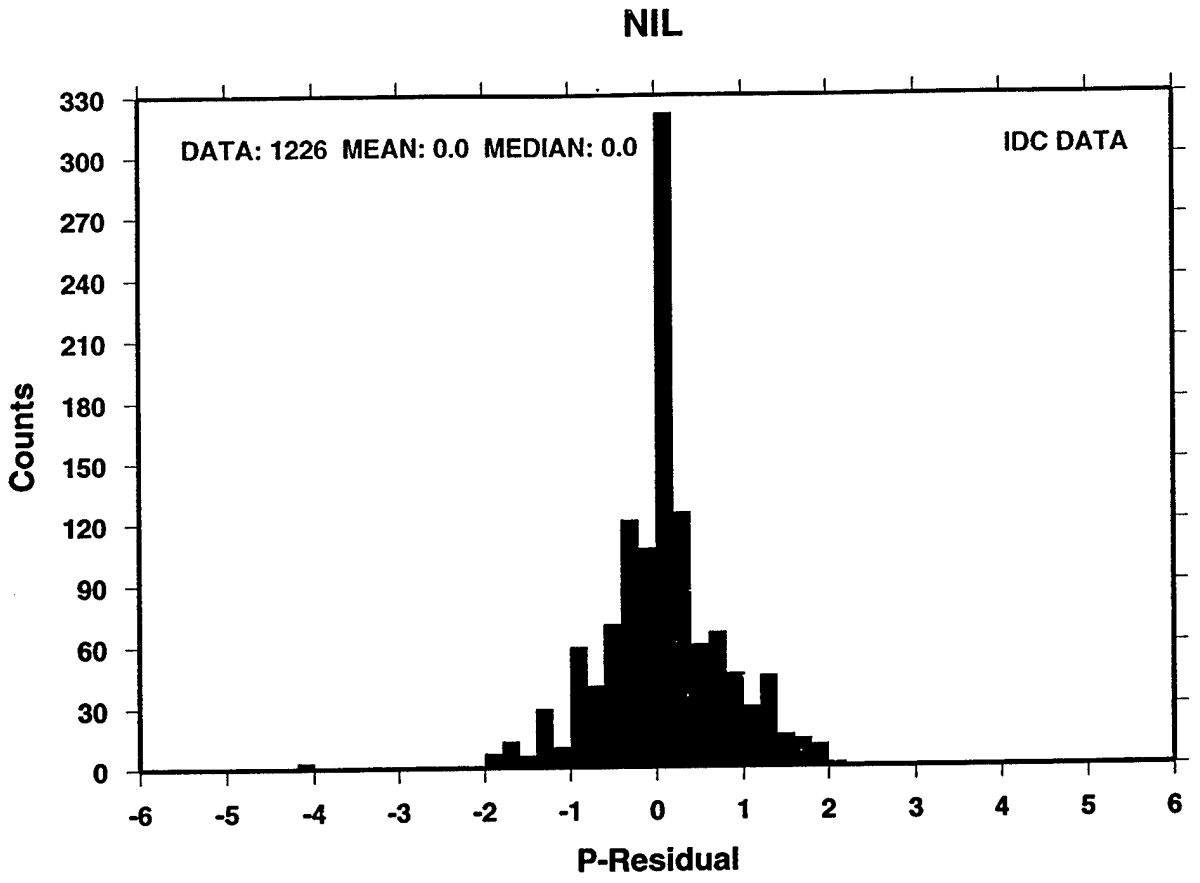
NIL
DATA: 1226 MEAN: 0.0 MEDIAN: 0.0
IDC DATA
Counts
330
300
270
240
210
180
150
120
90
60
30
0
-6
-5
-4
-3
-2
-1
0
1
2
3
4
5
6
P-Residual

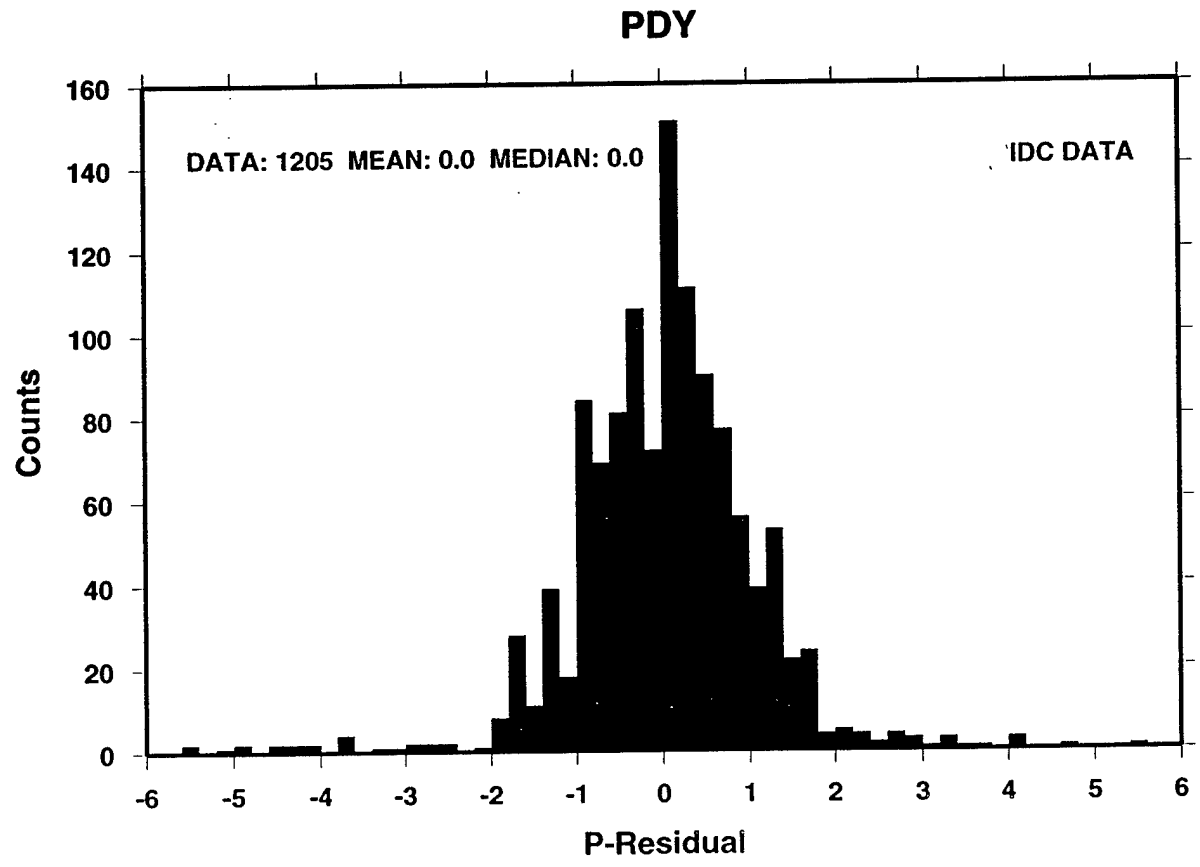
PDY
DATA: 1205 MEAN: 0.0 MEDIAN: 0.0
IDC DATA
Counts
160
140
120
100
80
60
40
20
0
-6
-5
-4
-3
-2
-1
0
1
2
3
4
5
6
P-Residual

Figure 8.

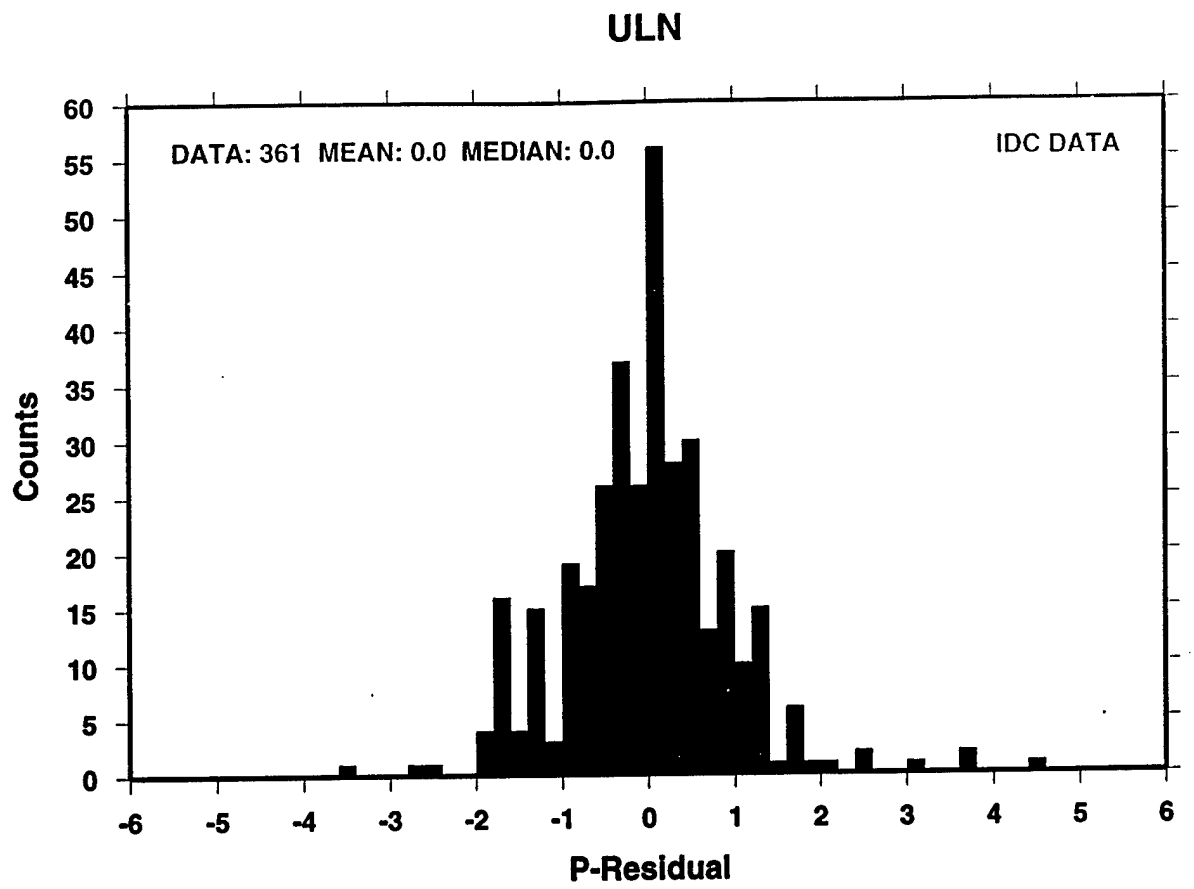
ULN
DATA: 361 MEAN: 0.0 MEDIAN: 0.0
IDC DATA
Counts
P-Residual
ZAL
DATA: 1575 MEAN: 1.1 MEDIAN: 0.6
IDC DATA
Counts
P-Residual

Figure 9.

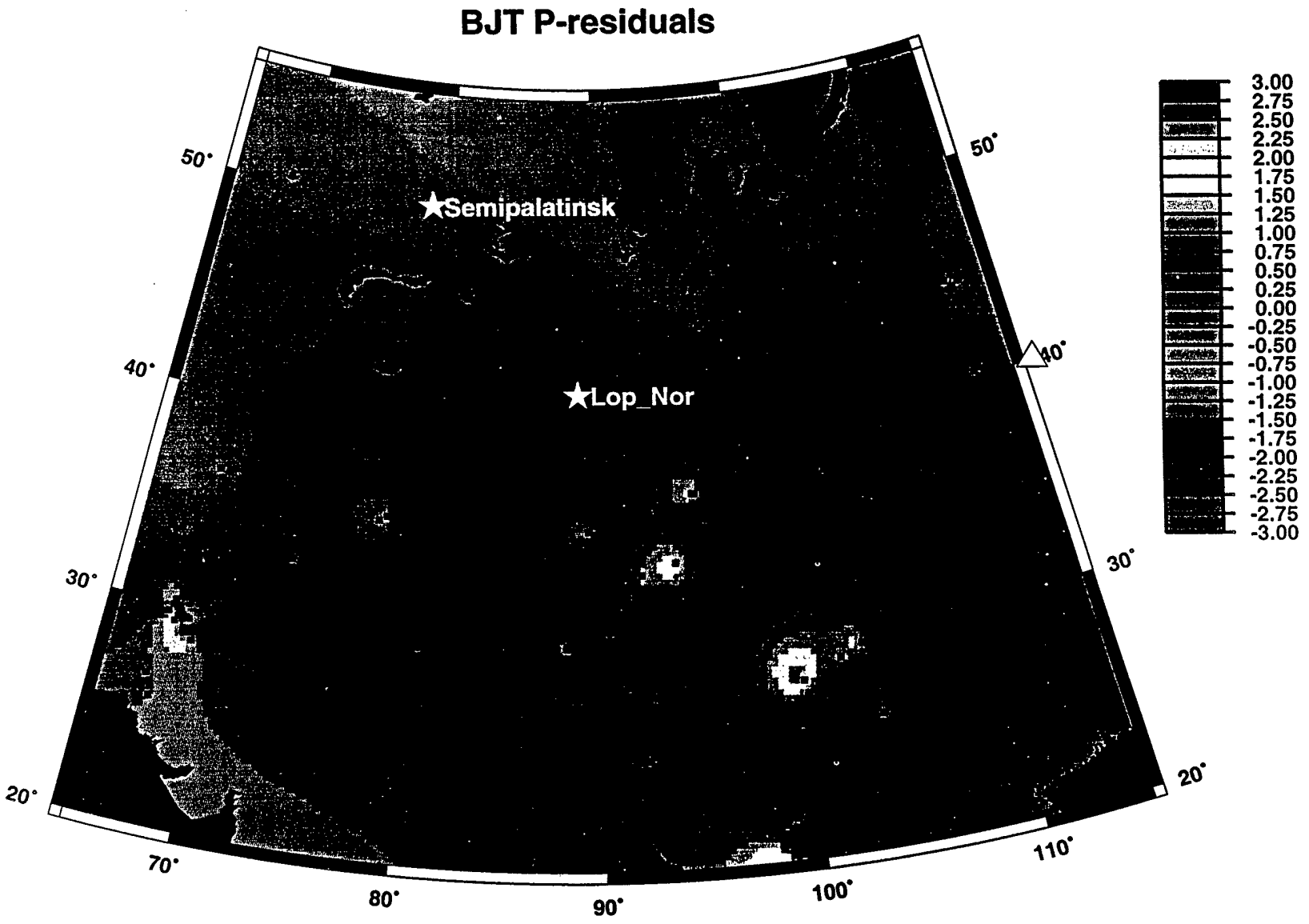
BJT P-residuals
Semipalatinsk
Lop_Nor
50°
40°
30°
20°
70°
80°
90°
100°
110°
3.00
2.75
2.50
2.25
2.00
1.75
1.50
1.25
1.00
0.75
0.50
0.25
0.00
-0.25
-0.50
-0.75
-1.00
-1.25
-1.50
-1.75
-2.00
-2.25
-2.50
-2.75
-3.00

Figure 10.

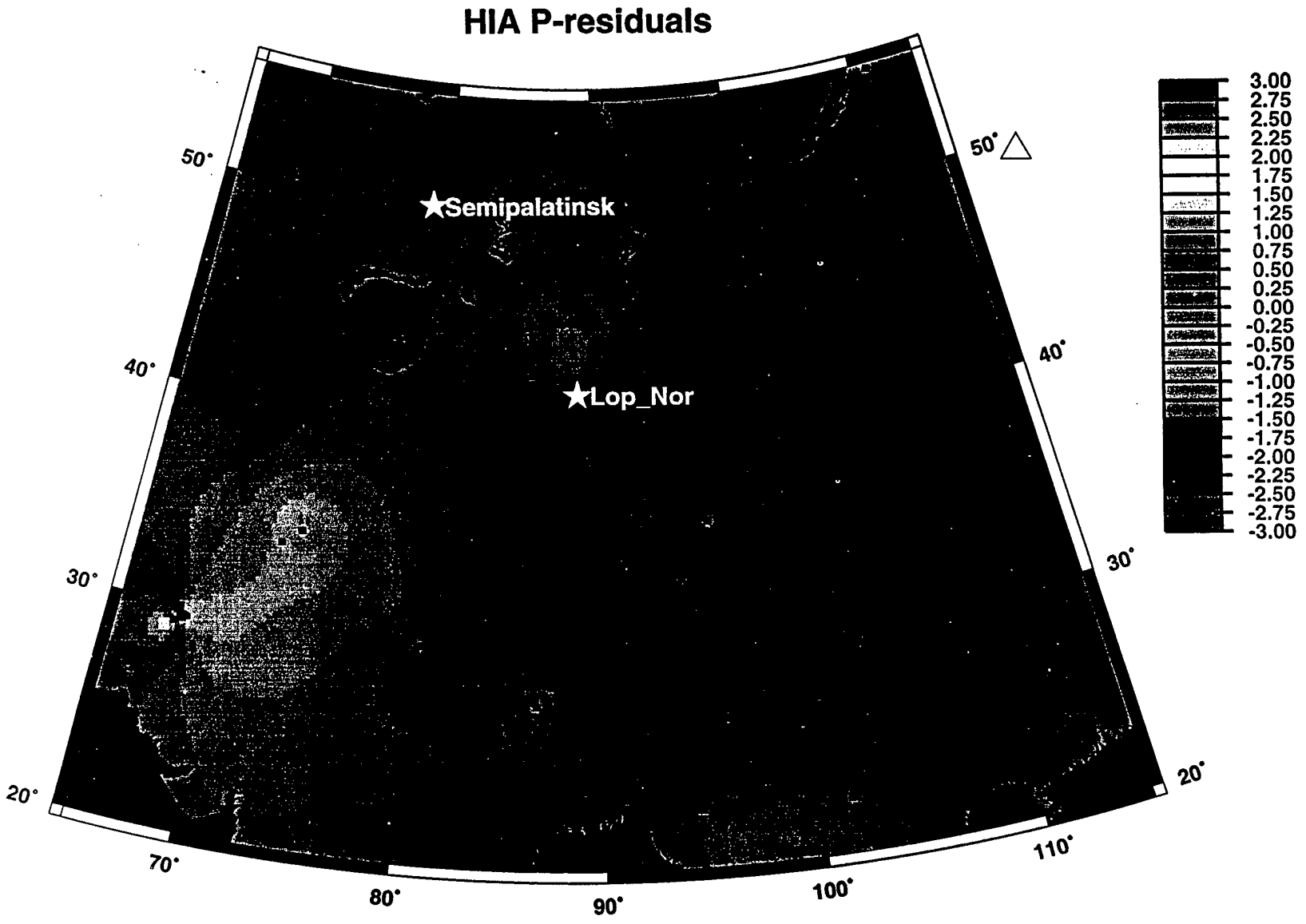
HIA P-residuals
Semipalatinsk
Lop_Nor
50°
40°
30°
20°
70°
80°
90°
100°
110°
3.00
2.75
2.50
2.25
2.00
1.75
1.50
1.25
1.00
0.75
0.50
0.25
0.00
-0.25
-0.50
-0.75
-1.00
-1.25
-1.50
-1.75
-2.00
-2.25
-2.50
-2.75
-3.00

Figure 11.

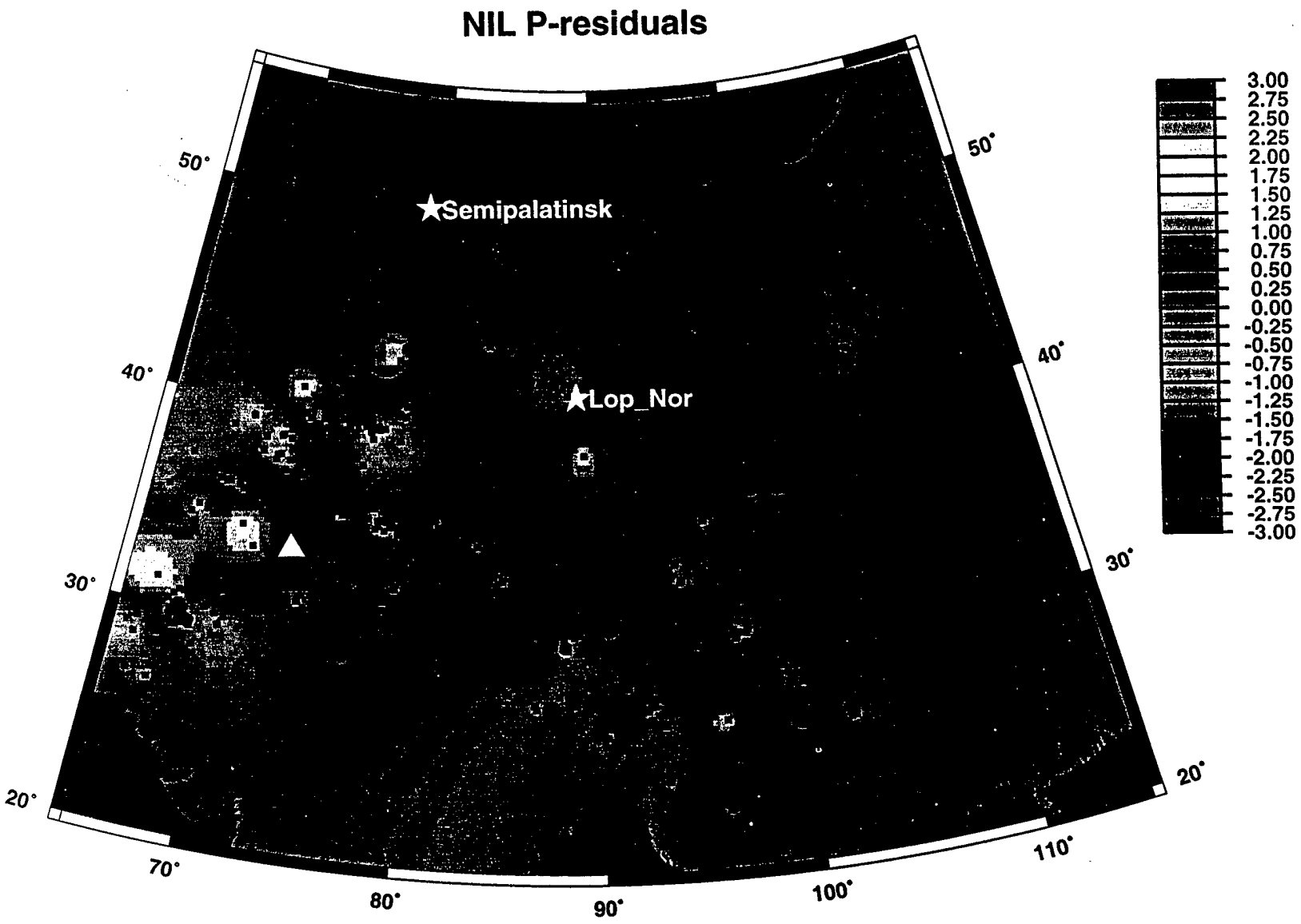
NIL P-residuals
Semipalatinsk
Lop_Nor
50°
40°
30°
20°
70°
80°
90°
100°
110°
3.00
2.75
2.50
2.25
2.00
1.75
1.50
1.25
1.00
0.75
0.50
0.25
0.00
-0.25
-0.50
-0.75
-1.00
-1.25
-1.50
-1.75
-2.00
-2.25
-2.50
-2.75
-3.00

Figure 12.

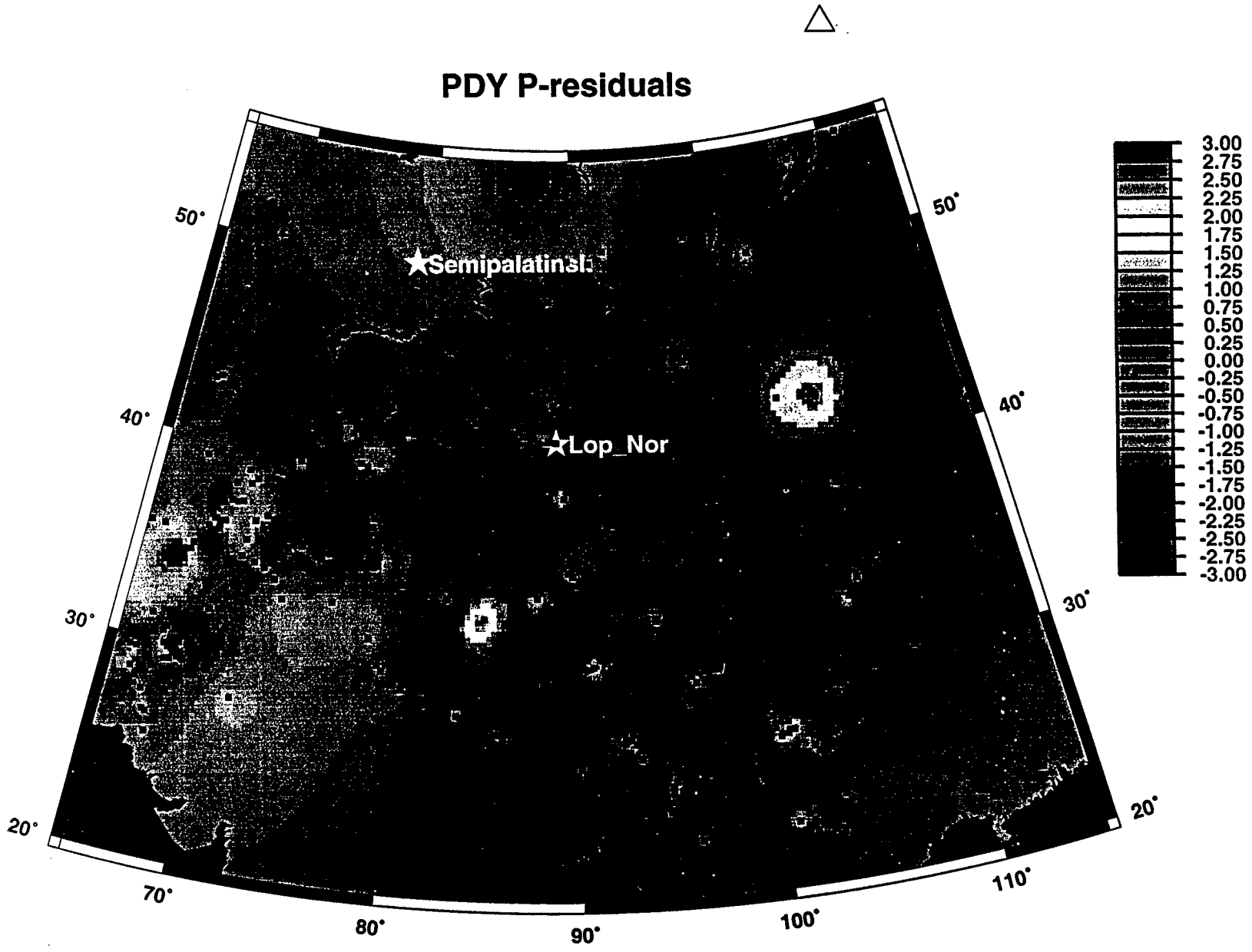
PDY P-residuals
Semipalatinsk
Lop_Nor
50°
40°
30°
20°
70°
80°
90°
100°
110°
3.00
2.75
2.50
2.25
2.00
1.75
1.50
1.25
1.00
0.75
0.50
0.25
0.00
-0.25
-0.50
-0.75
-1.00
-1.25
-1.50
-1.75
-2.00
-2.25
-2.50
-2.75
-3.00

Figure 13.

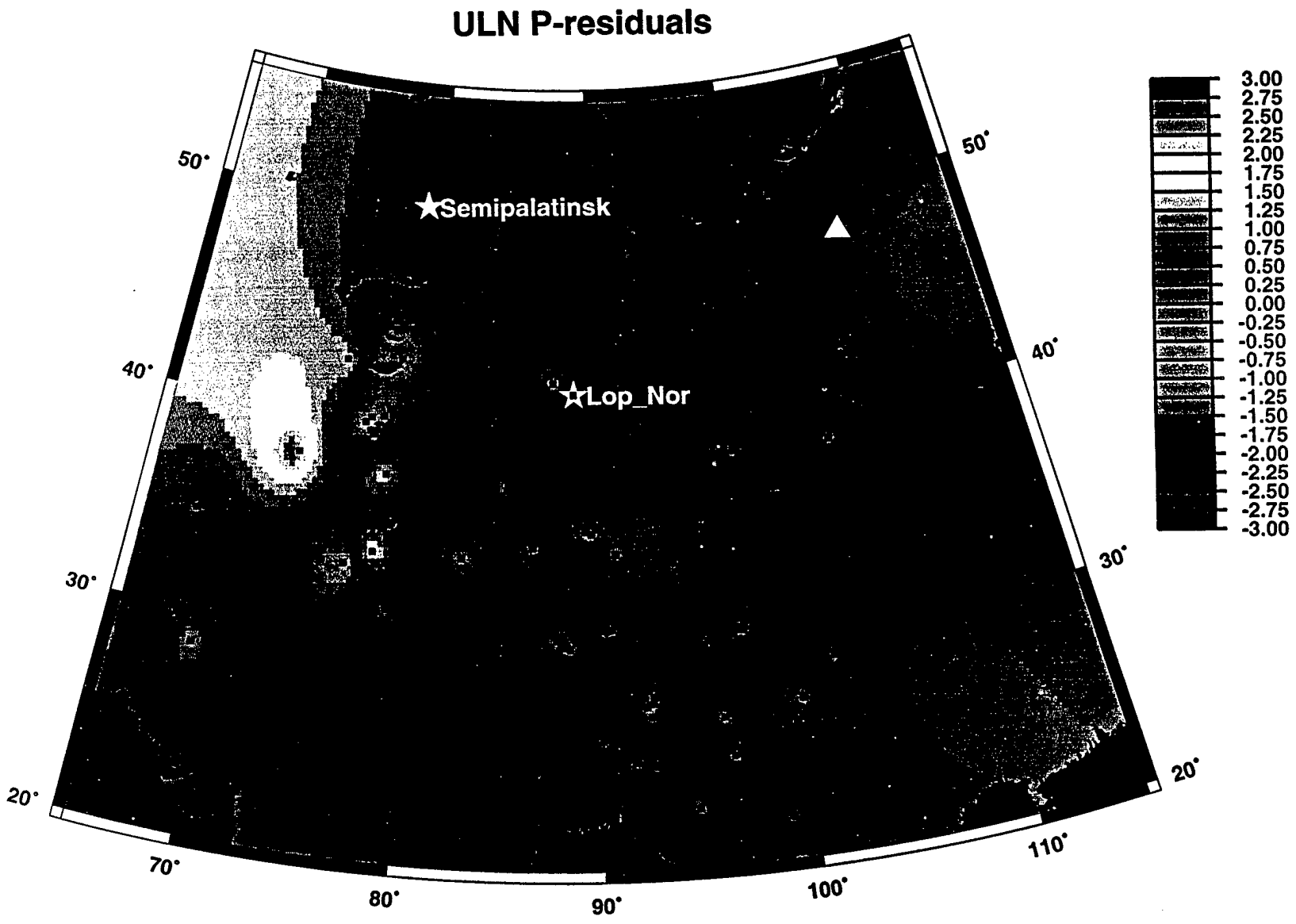
ULN P-residuals
Semipalatinsk
Lop_Nor
50°
40°
30°
20°
70°
80°
90°
100°
110°
3.00
2.75
2.50
2.25
2.00
1.75
1.50
1.25
1.00
0.75
0.50
0.25
0.00
-0.25
-0.50
-0.75
-1.00
-1.25
-1.50
-1.75
-2.00
-2.25
-2.50
-2.75
-3.00

Figure 14.

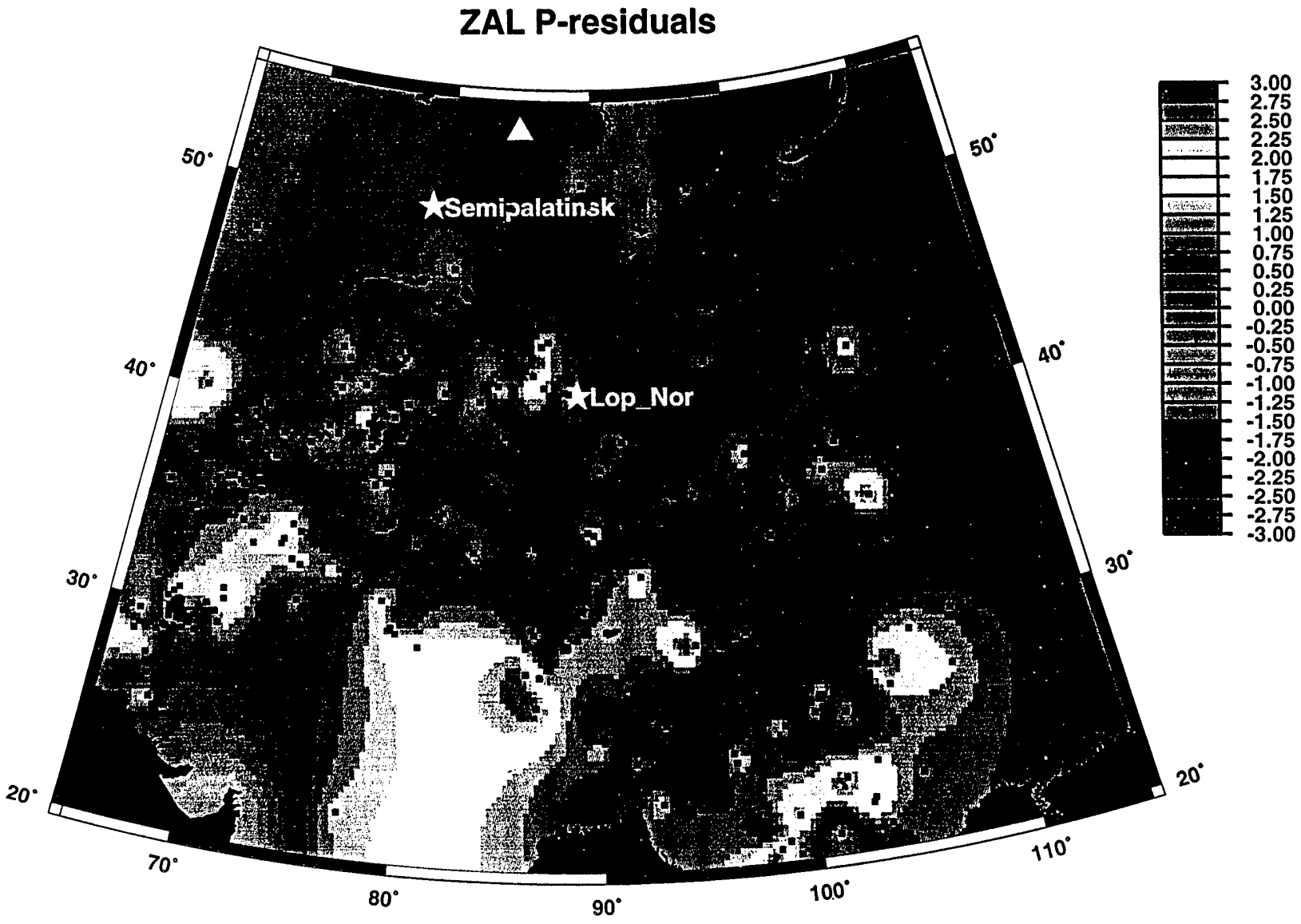
ZAL P-residuals
Semipalatinsk
Lop_Nor
50°
40°
30°
20°
70°
80°
90°
100°
110°
3.00
2.75
2.50
2.25
2.00
1.75
1.50
1.25
1.00
0.75
0.50
0.25
0.00
-0.25
-0.50
-0.75
-1.00
-1.25
-1.50
-1.75
-2.00
-2.25
-2.50
-2.75
-3.00

Figure 15.

Errors in Location of Chinese Nuclear Events

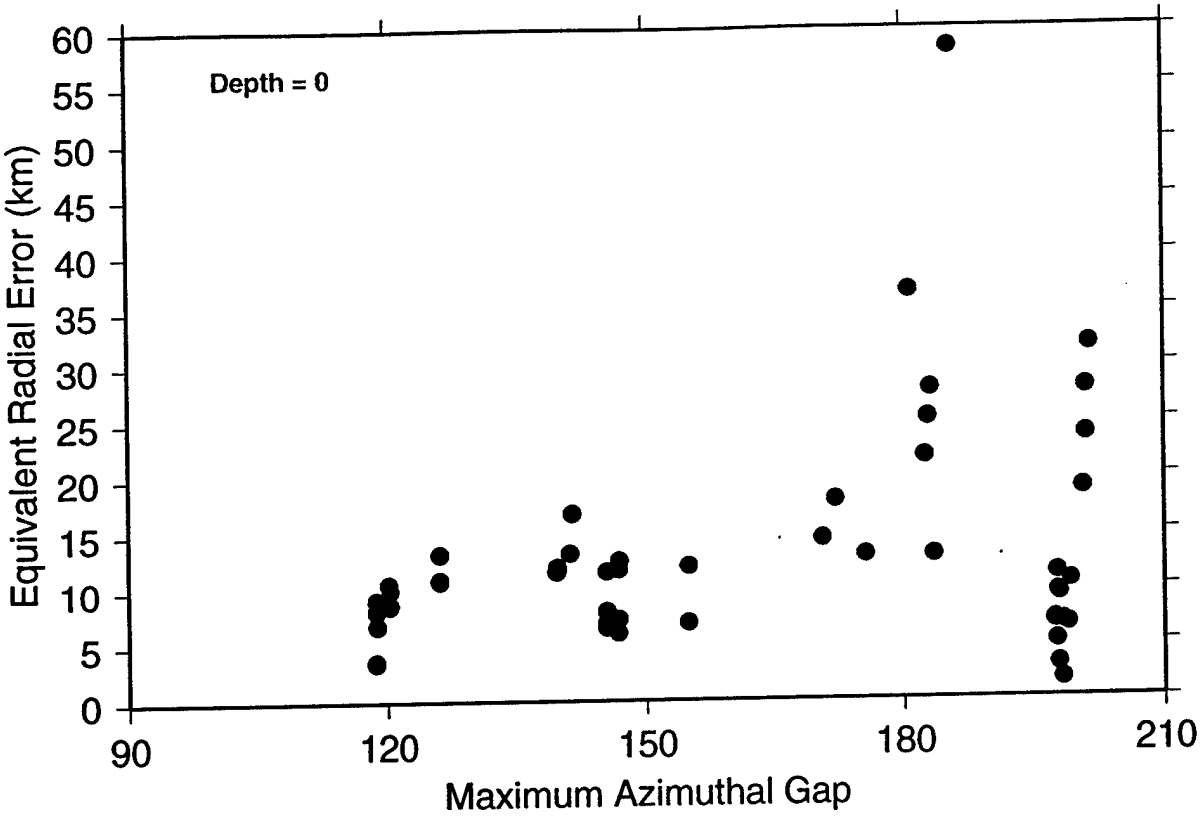

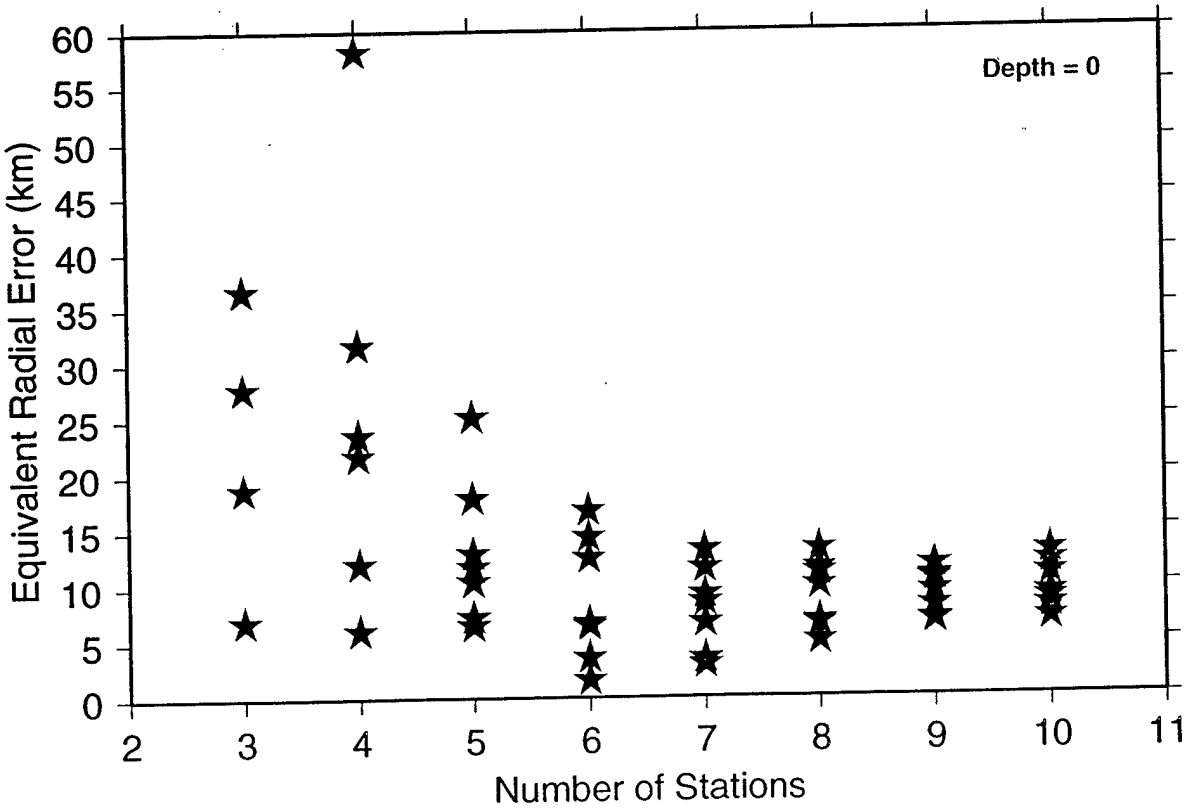

Figure 16.

Errors in Location of Chinese Nuclear Events

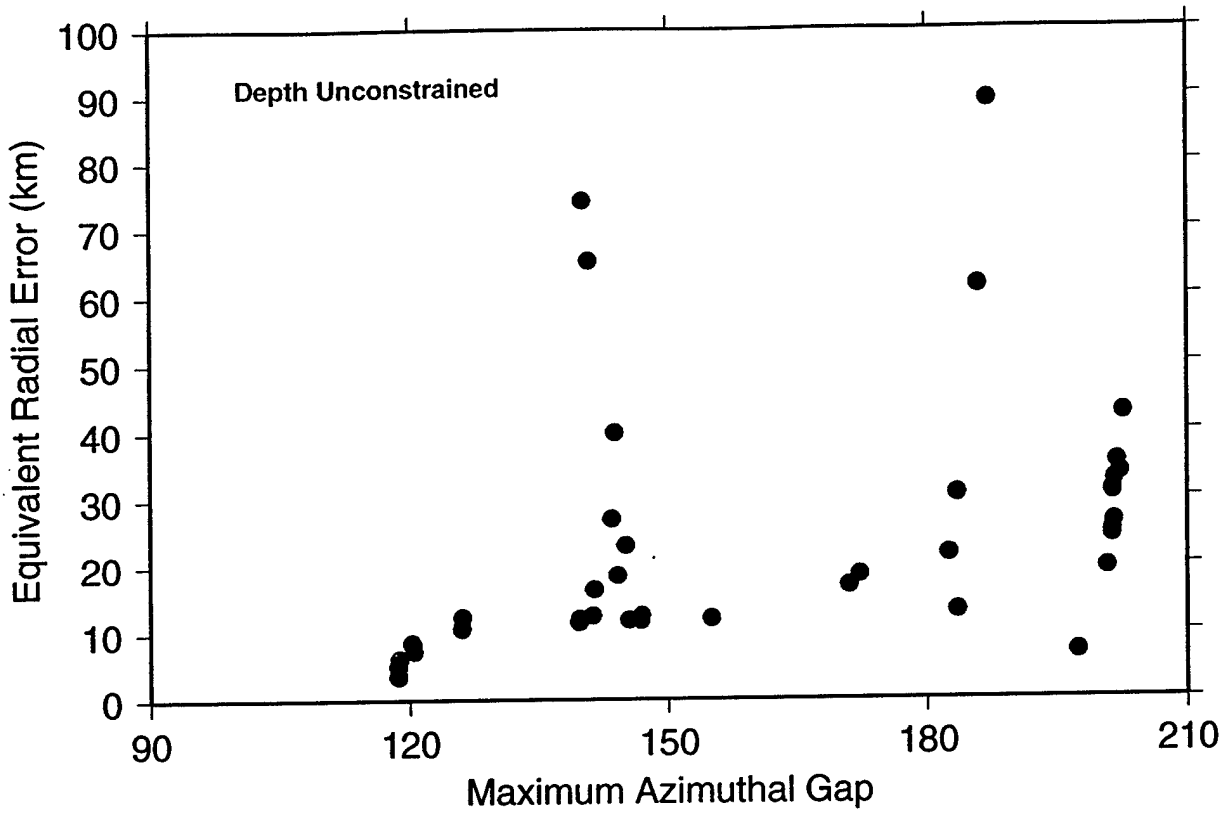

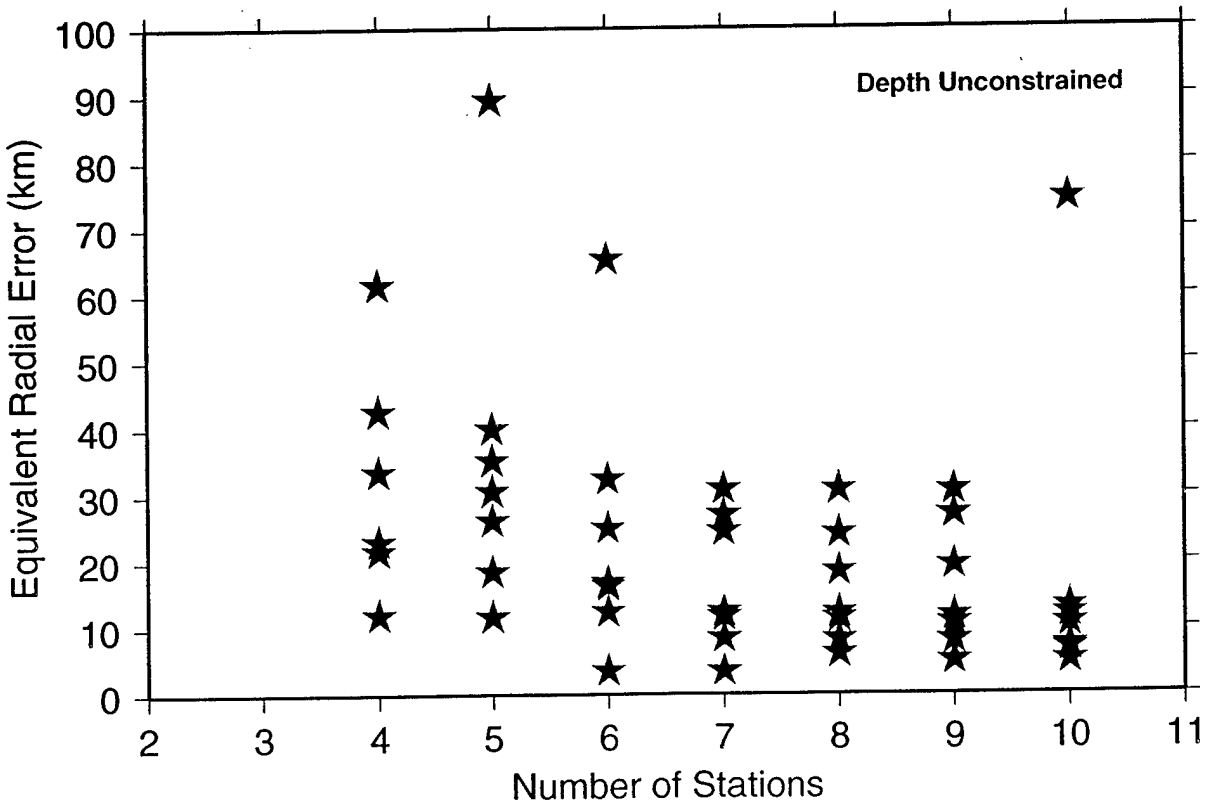

Figure 17.

Errors in Location of Chinese Nuclear Events

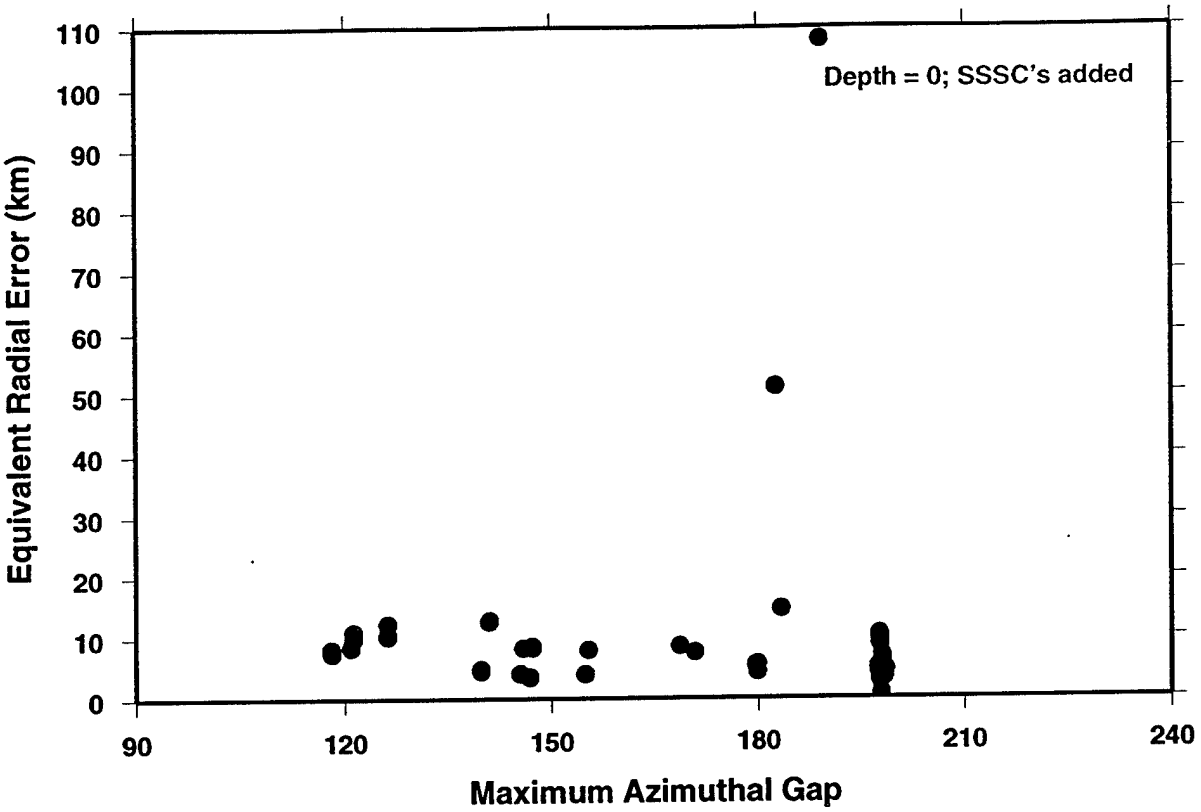

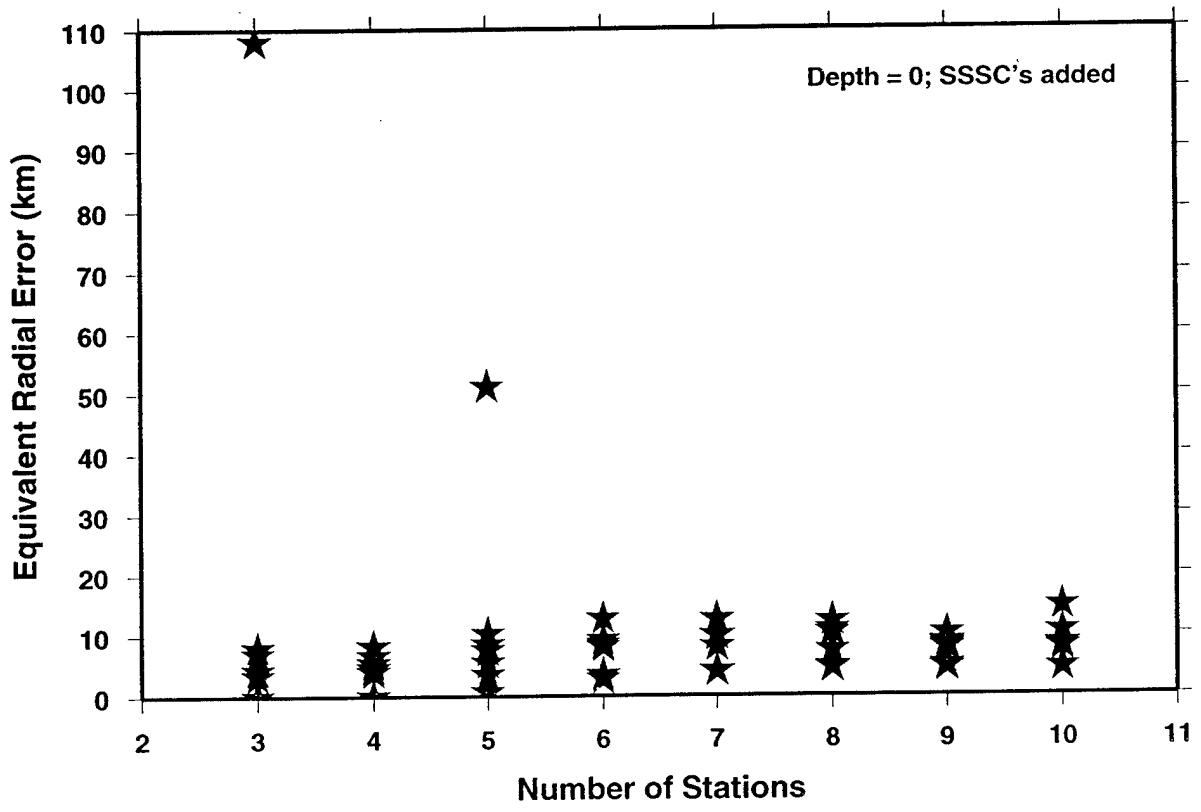

Figure 18.

Errors in Location of Chinese Nuclear Events

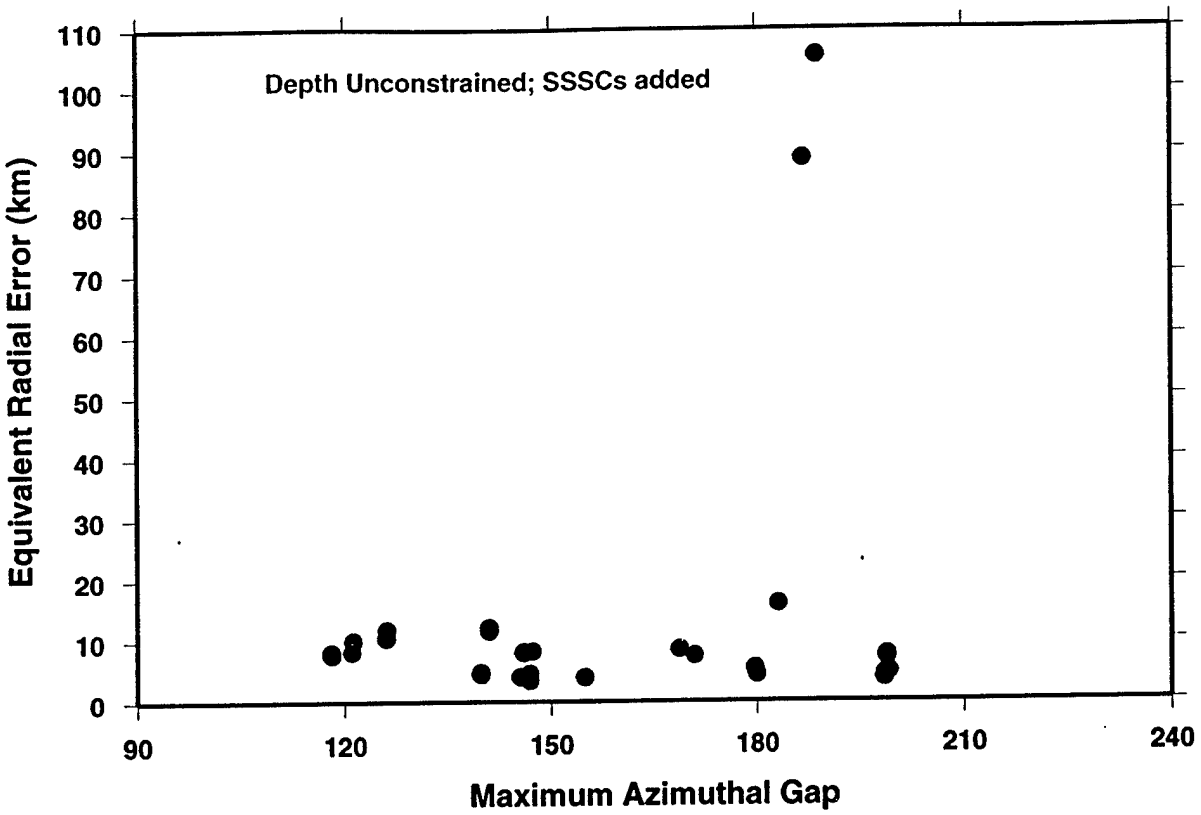

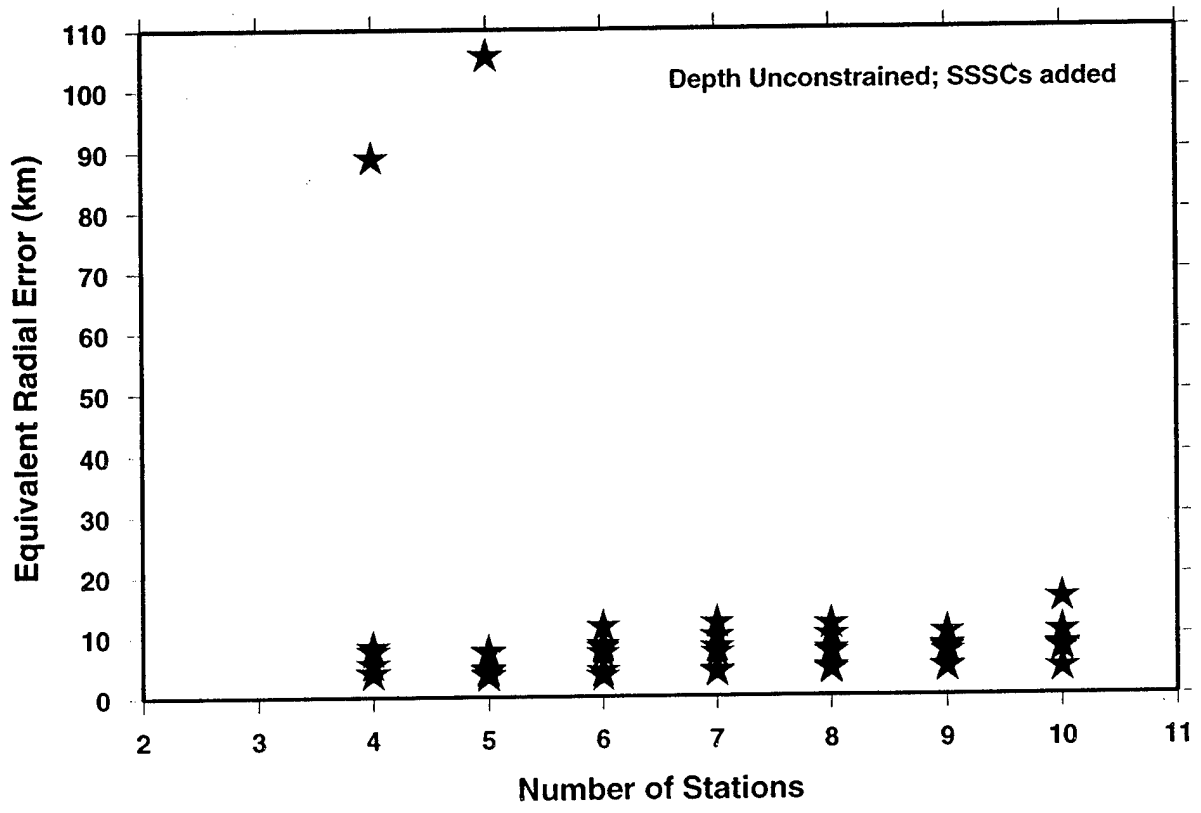

Figure 19.

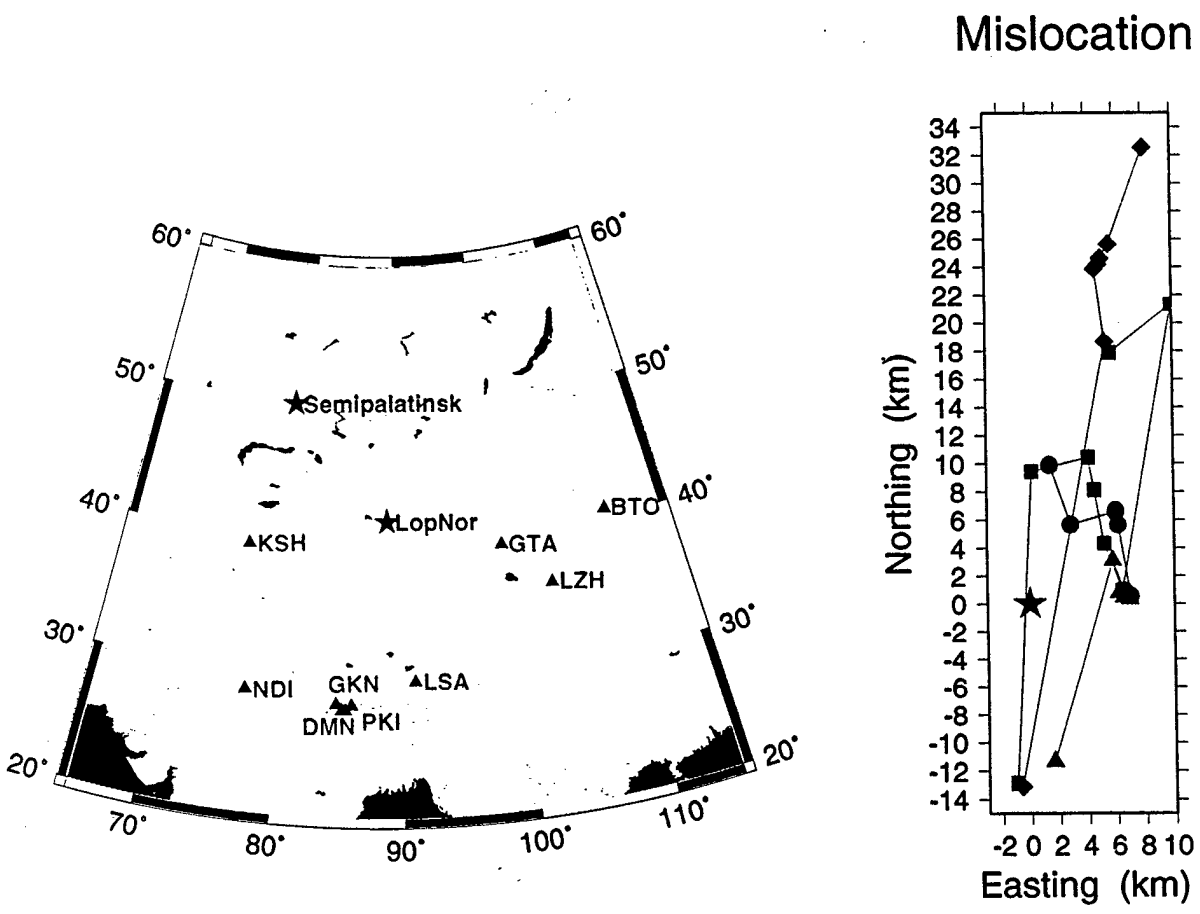

Figure 20. Station Distribution and Mislocations for the Chinese Event of May 1990

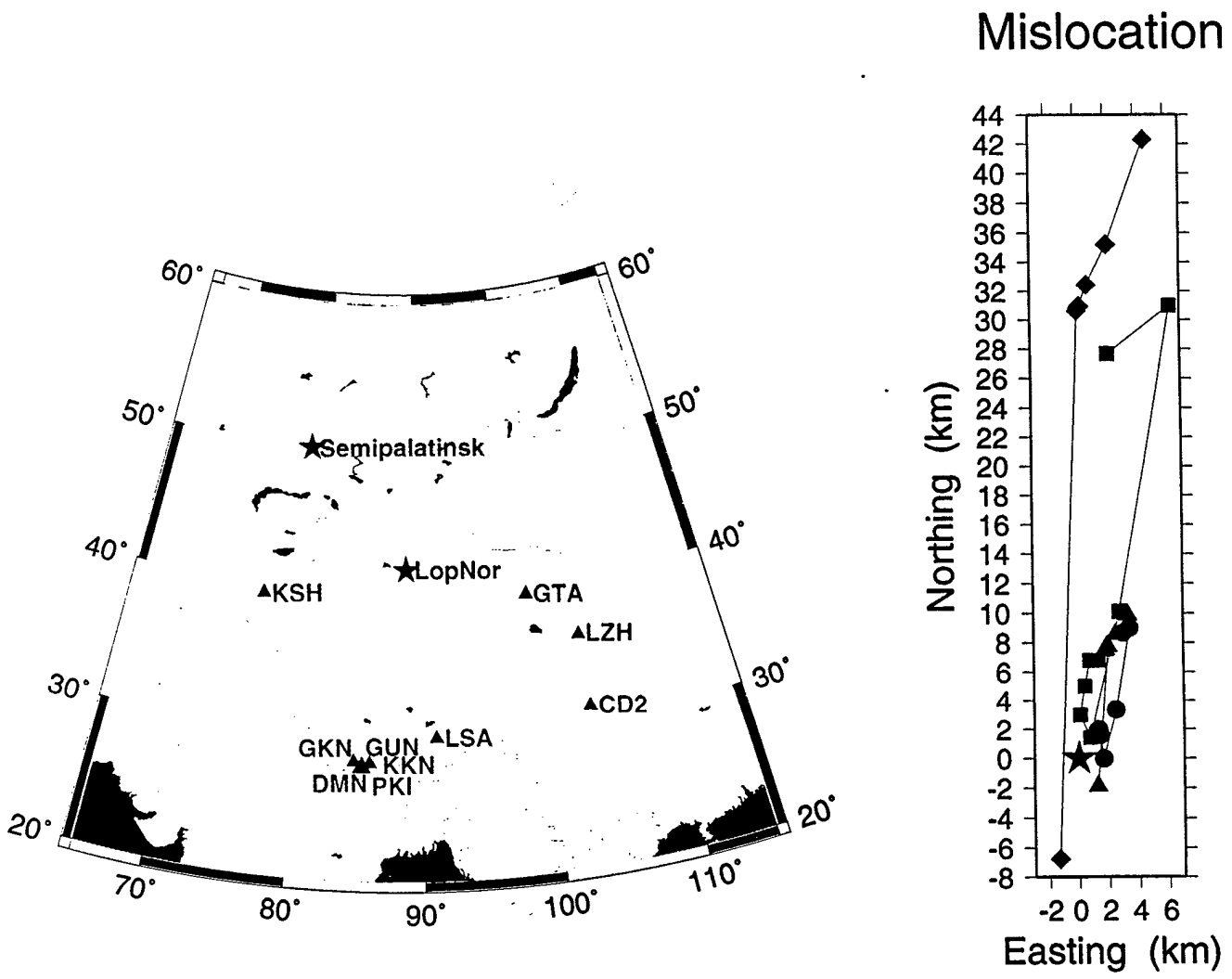

Figure 21. Station Distribution and Mislocations for the Chinese Event of August 1990

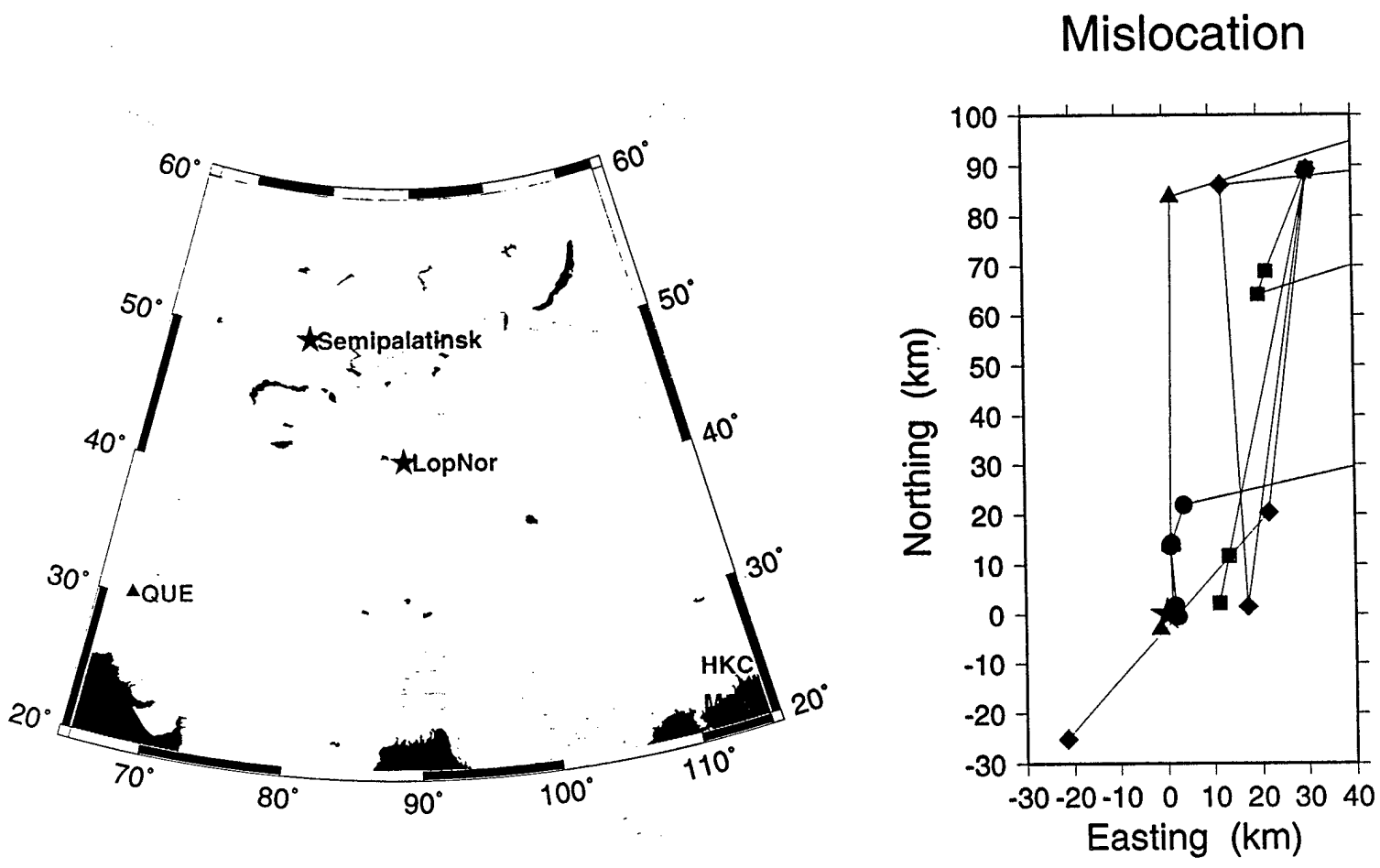

Figure 22. Station Distribution and Mislocations for the Chinese Event of May 1992

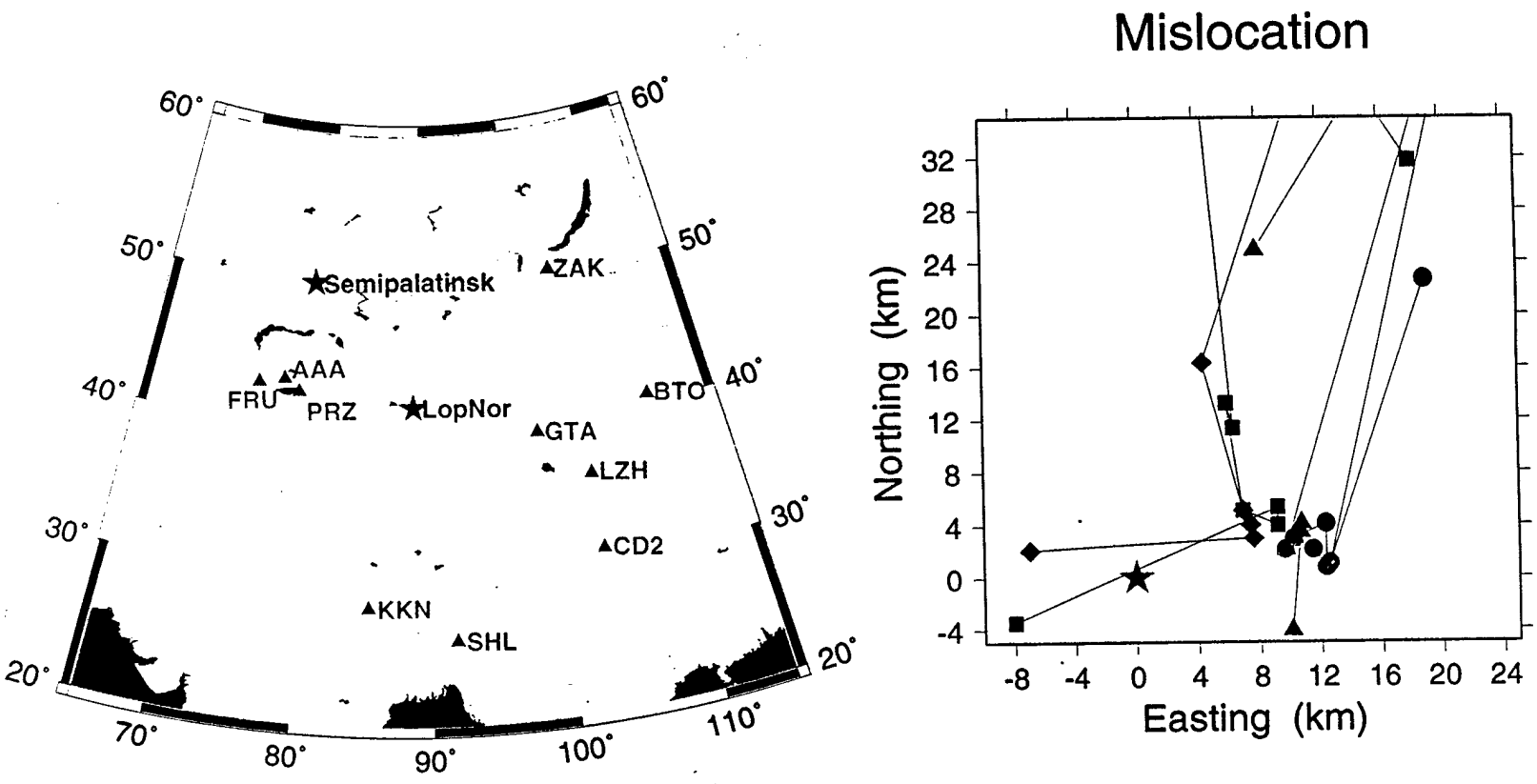

Figure 23. Station Distribution and Mislocations for the Chinese Event of September 1992

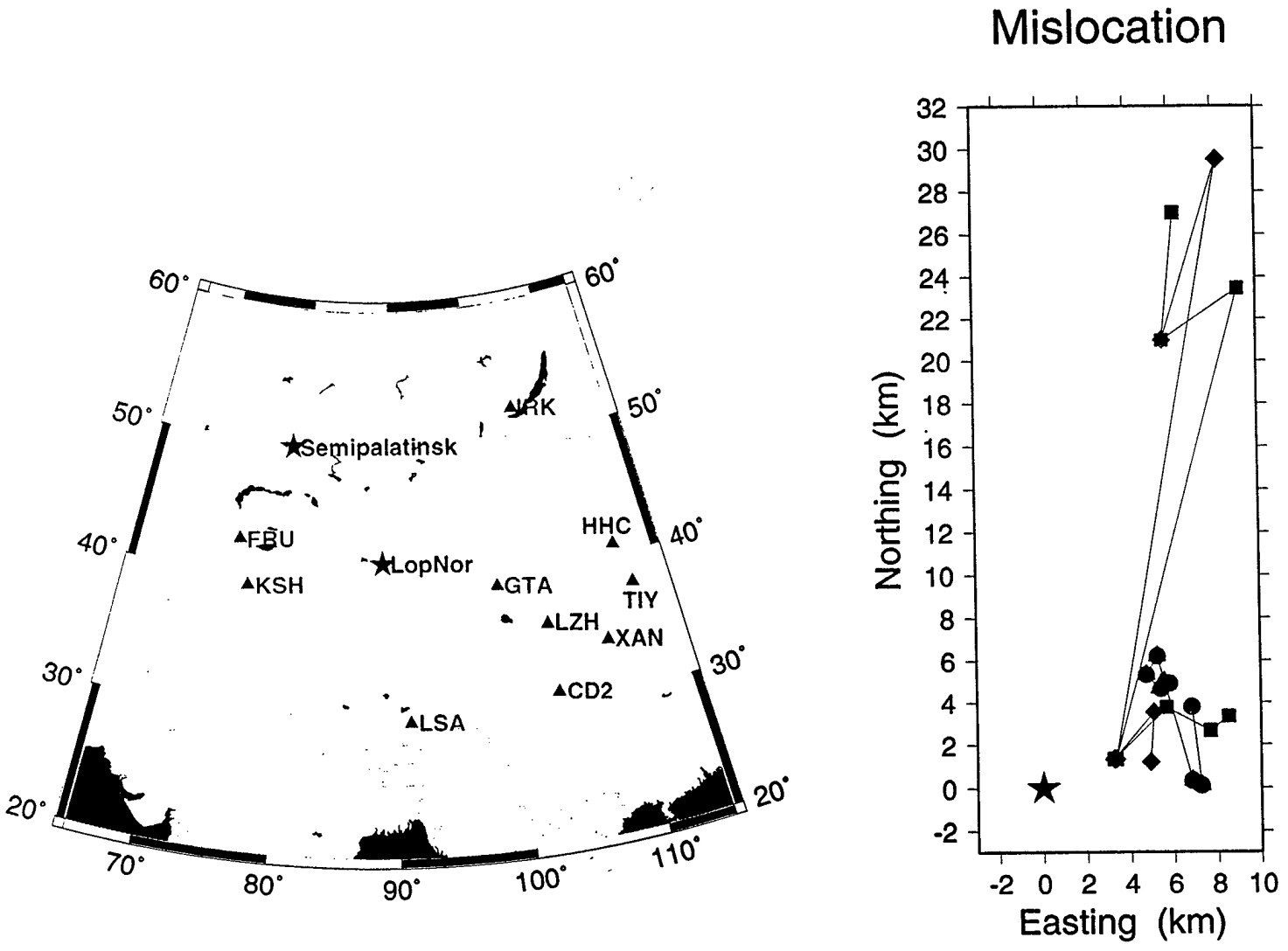

Figure 24. Station Distribution and Mislocations for the Chinese Event of October 1993

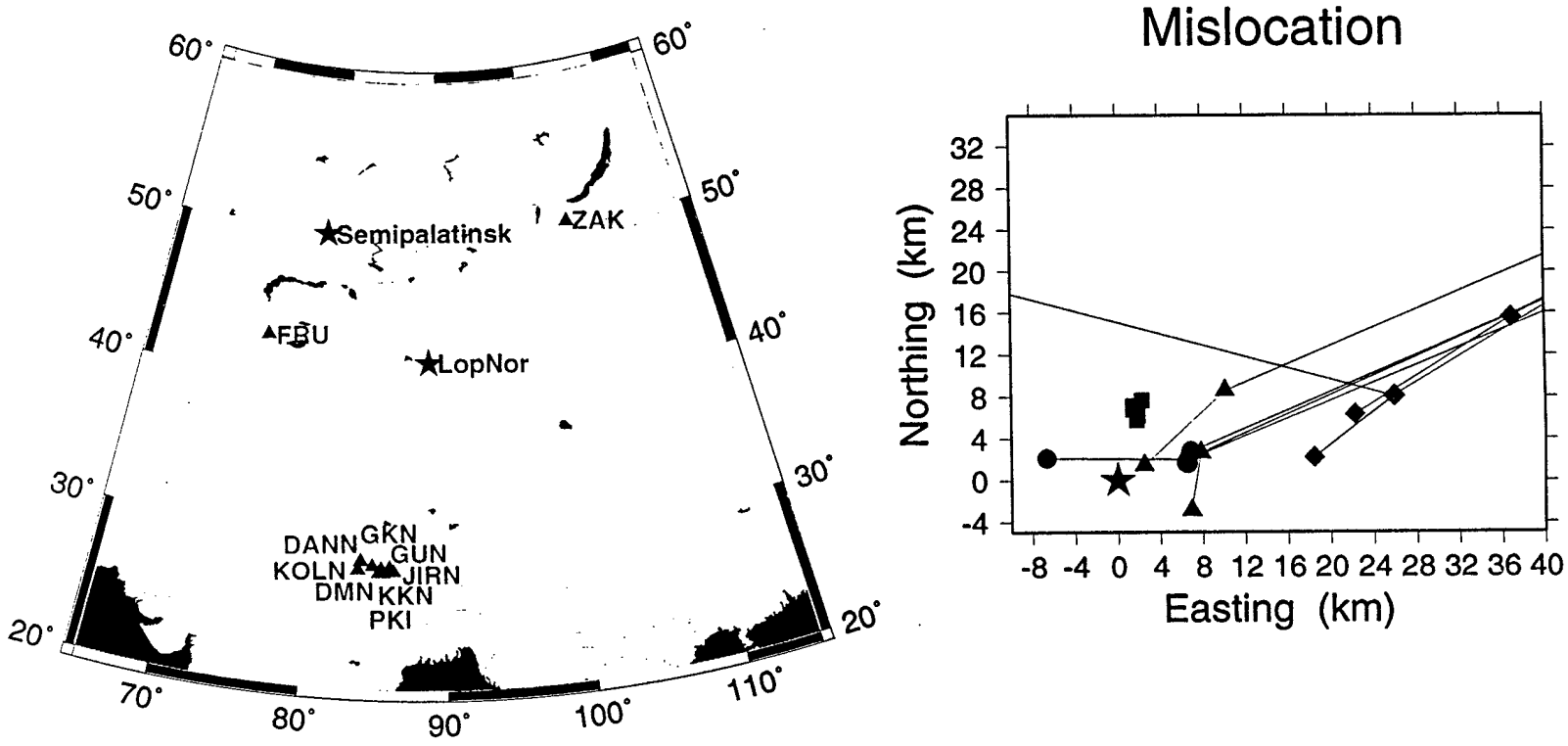

Figure 25. Station Distribution and Mislocations for the Chinese Event of June 1994

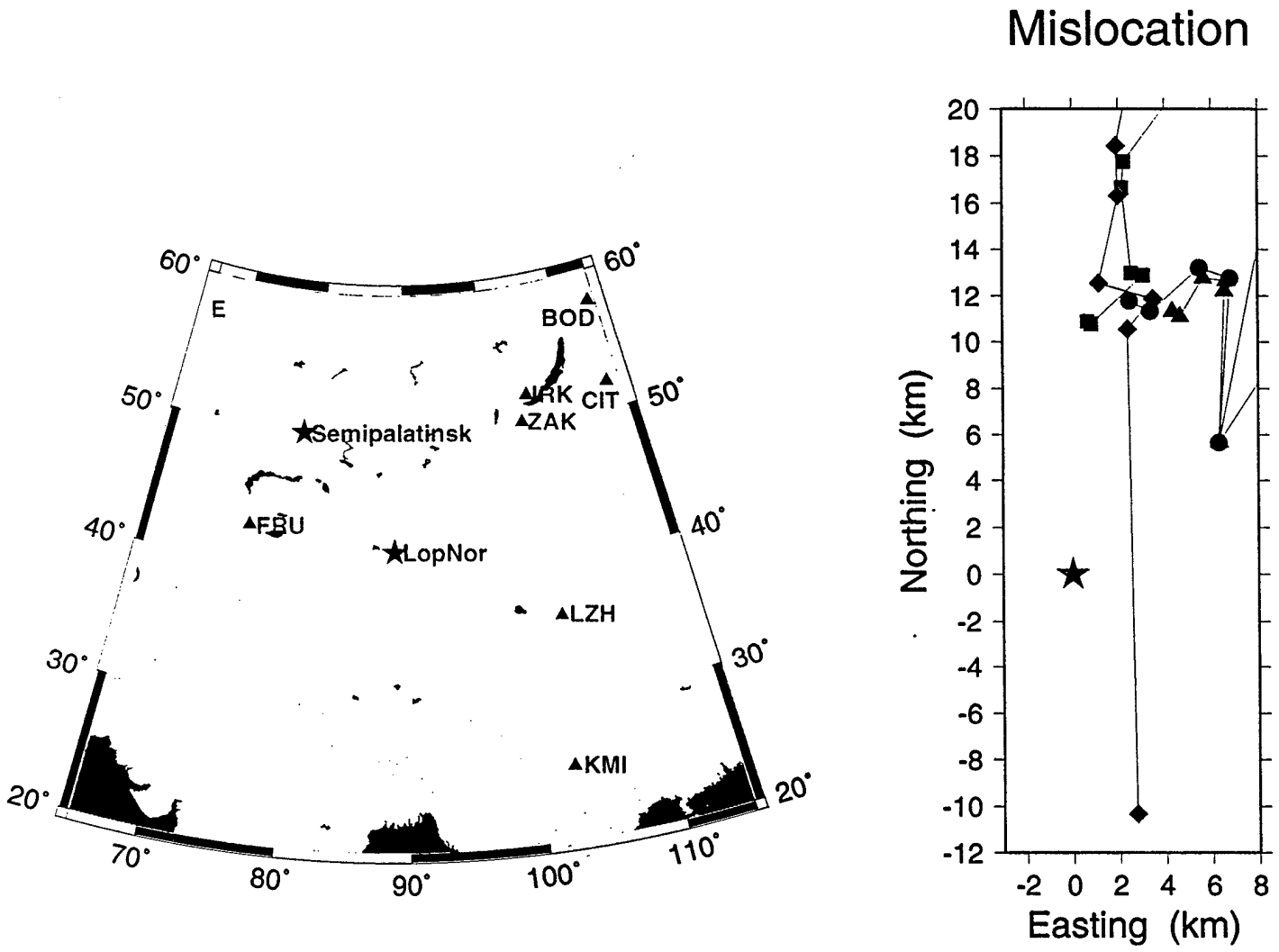

Figure 26. Station Distribution and Mislocations for the Chinese Event of October 1994

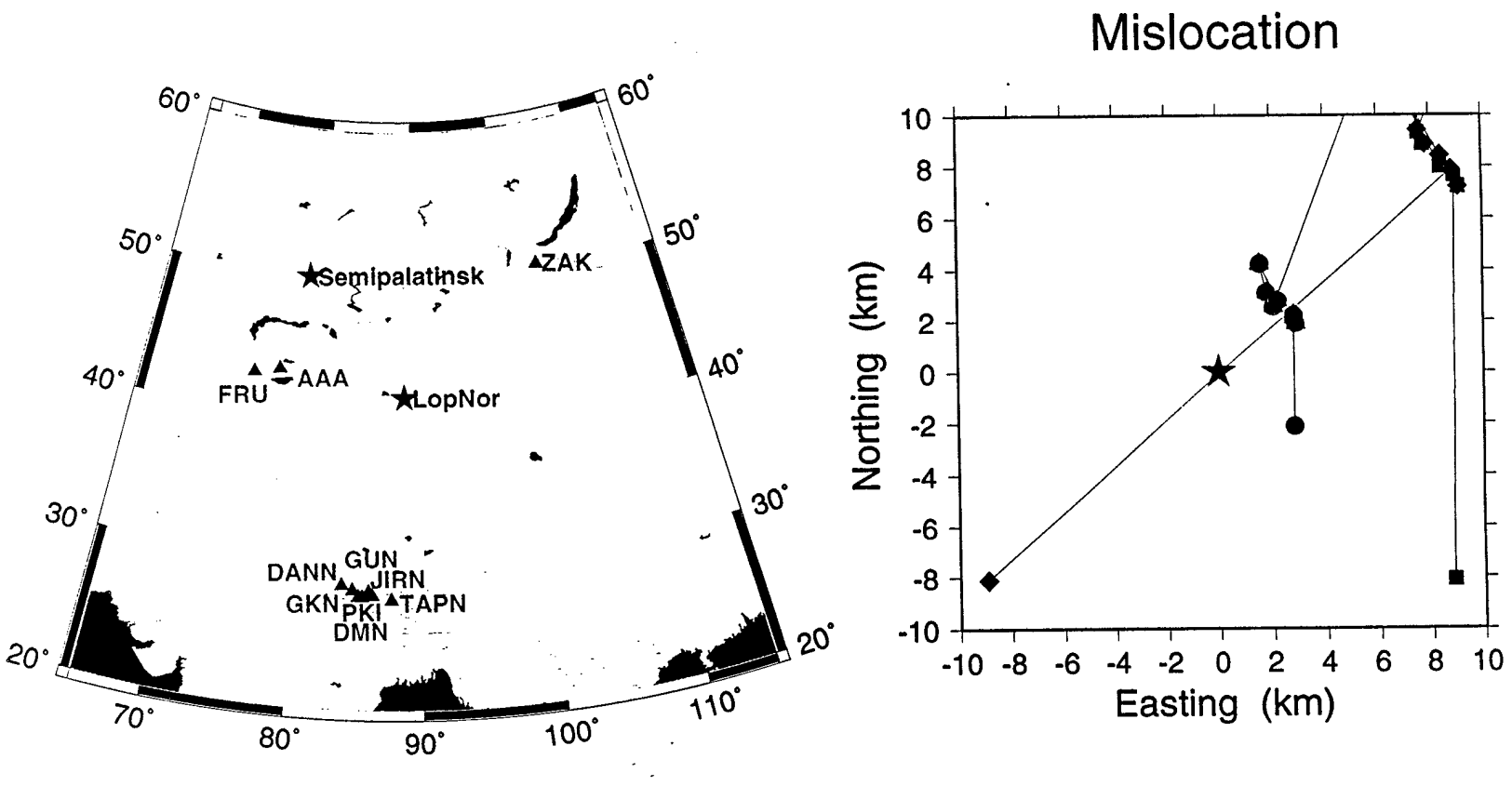

Figure 27. Station Distribution and Mislocations for the Chinese Event of August 1995

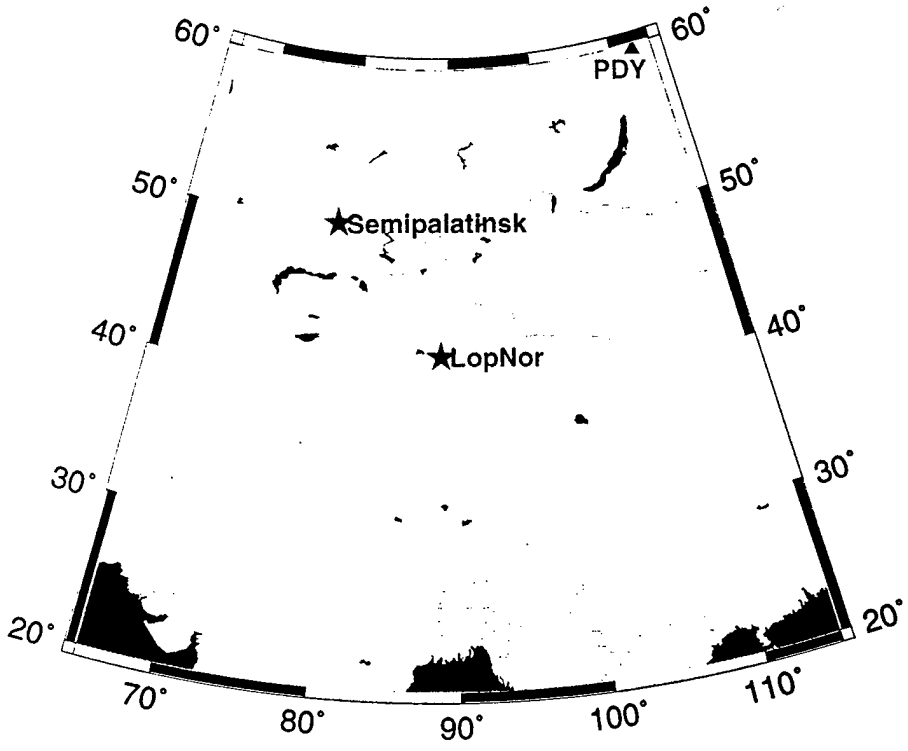

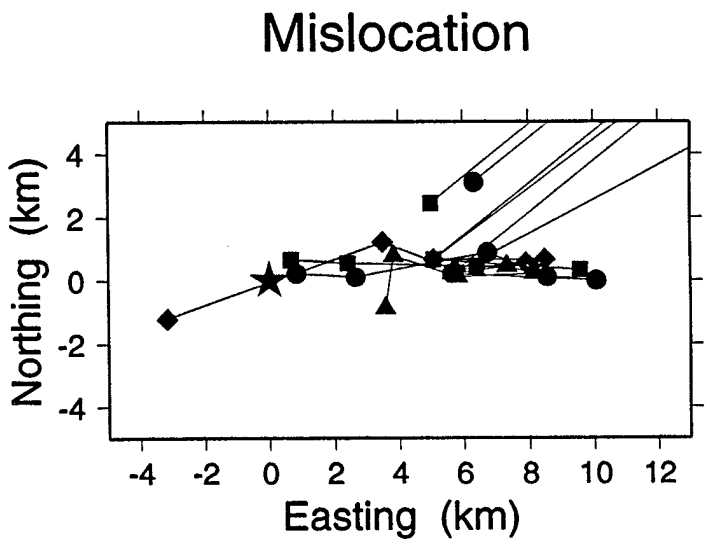

Figure 28. Station Distribution and Mislocations for the Chinese Event of June 1996

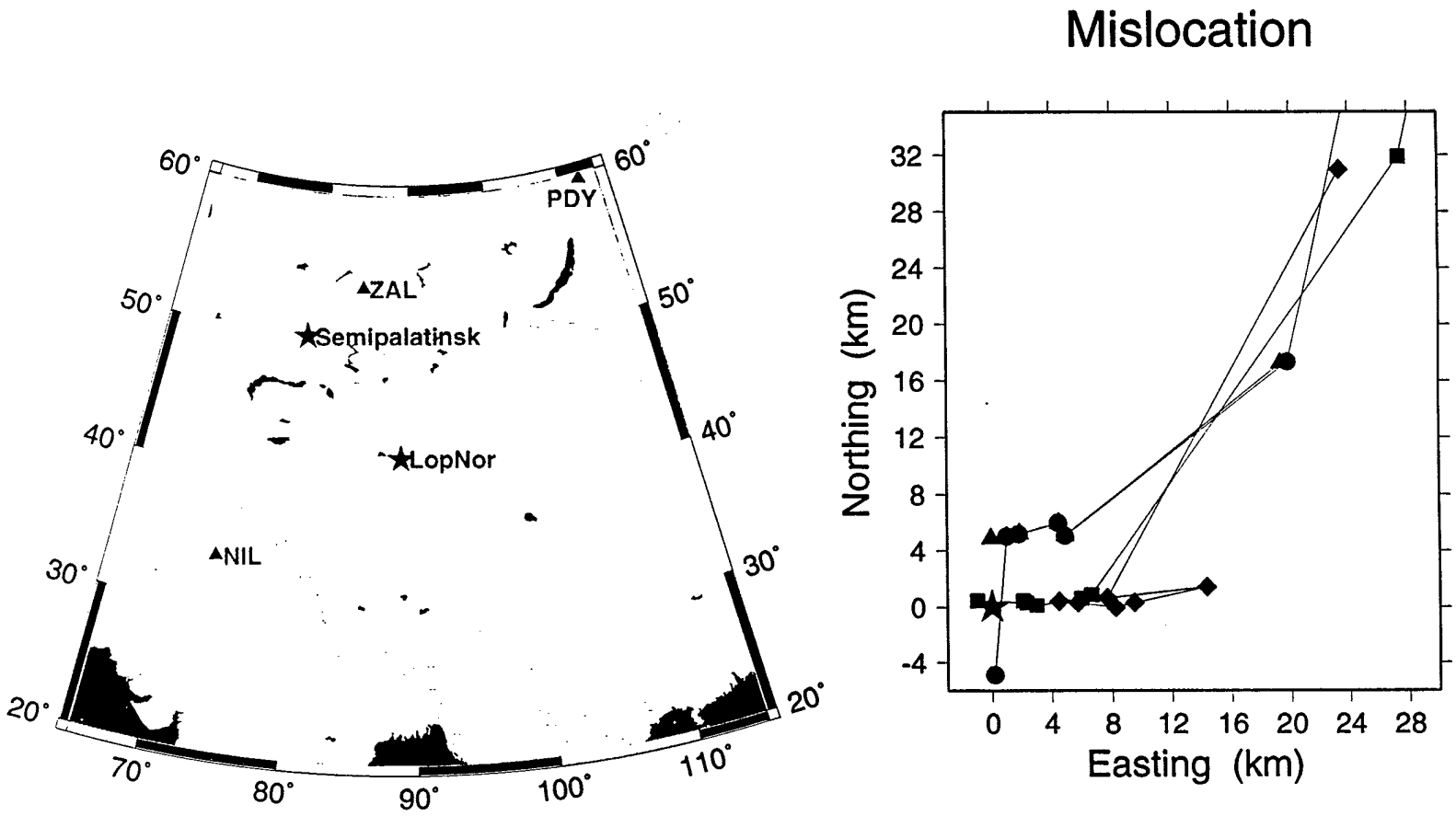

Figure 29. Station Distribution and Mislocations for the Chinese Event of July 1996

Errors in Location of Kyrgyzstan Aftershock

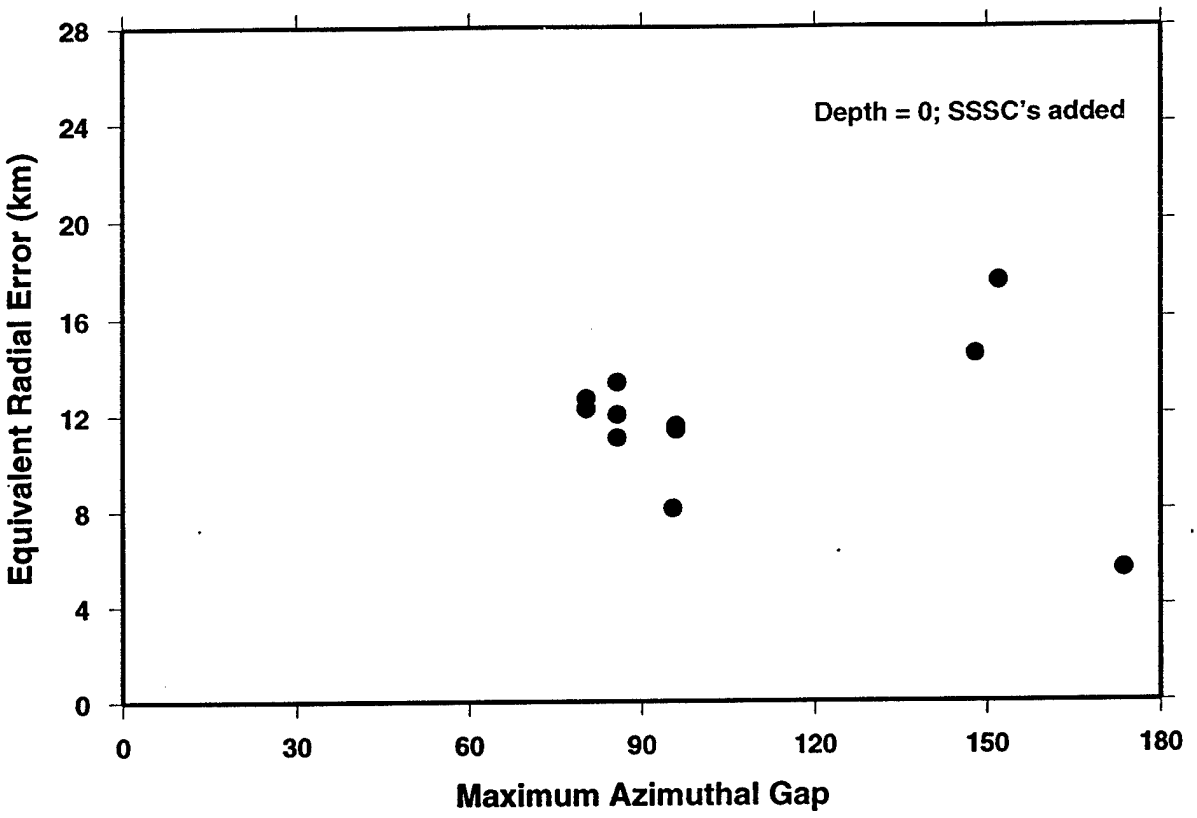

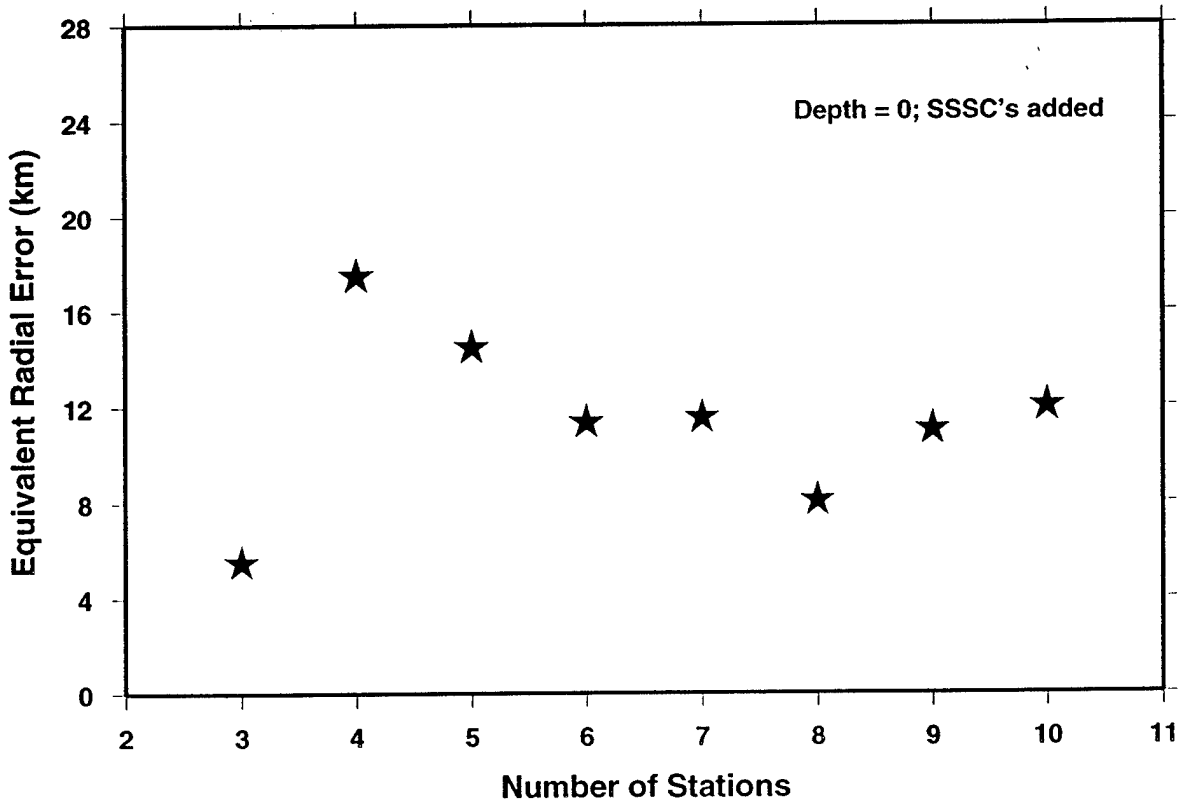

Figure 30.

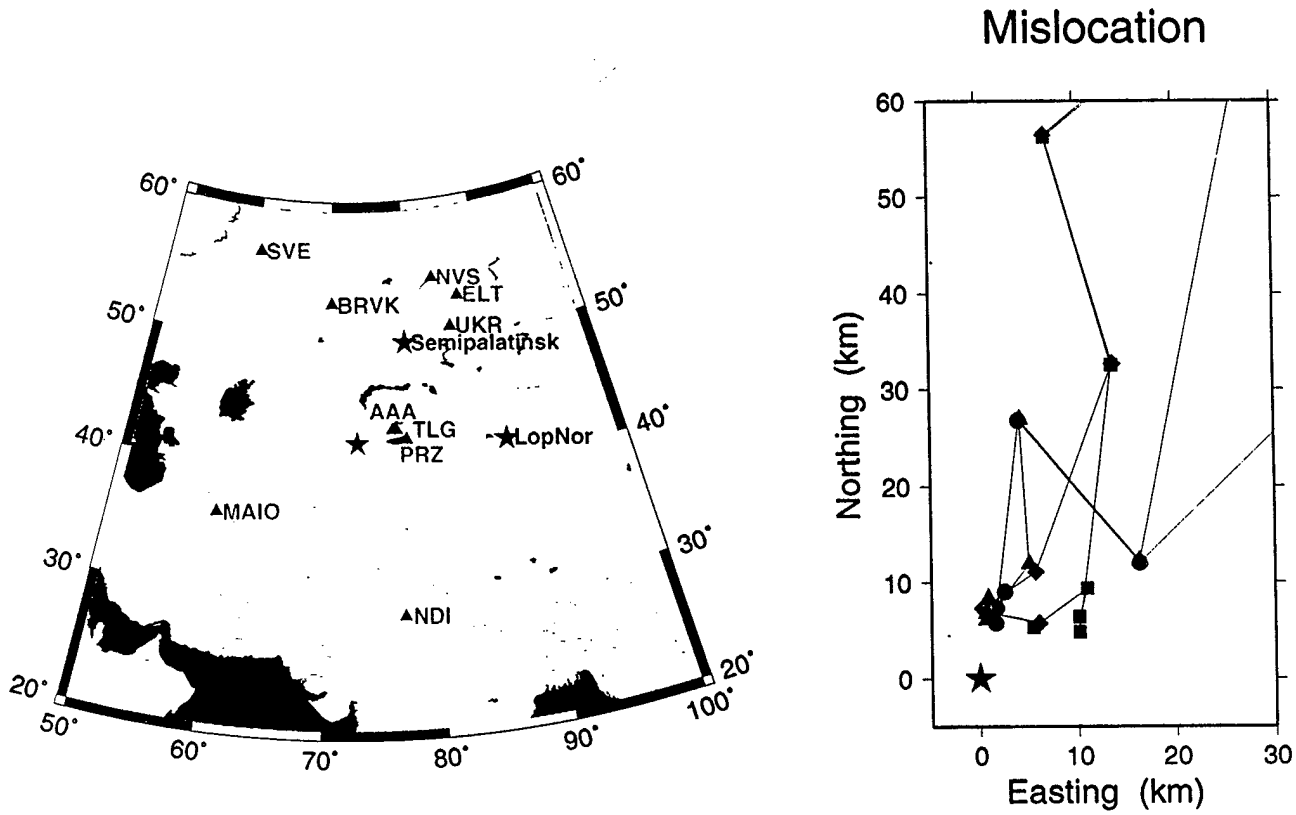

Figure 31. Station Distribution and Mislocations for a Kyrgyzstan Earthquake in 1992

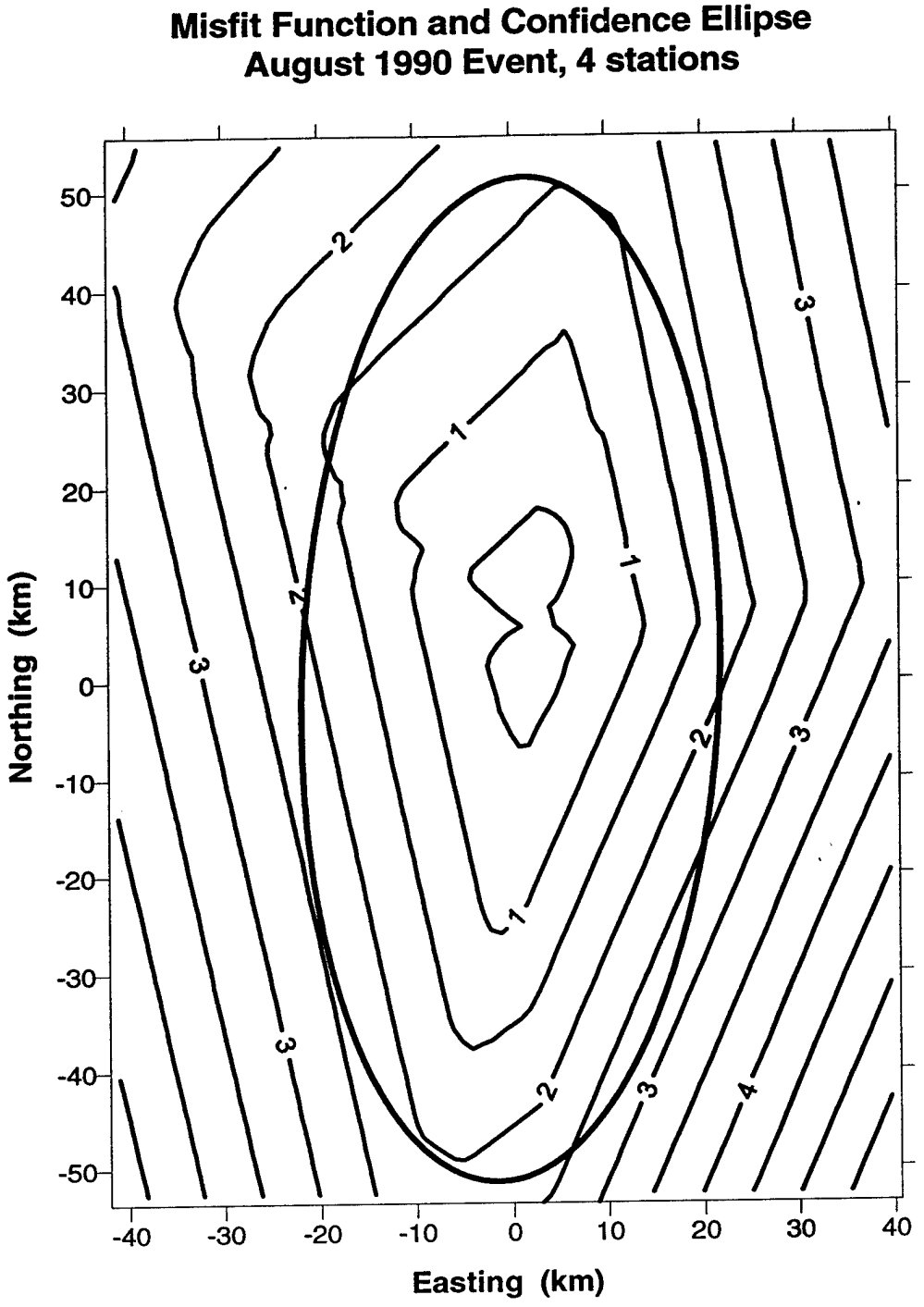

Fig. 32. Contours of the misfit function for the August 1990 Chinese Event. The uncertainty ellipse calculated by LocSAT is shown for comparison.

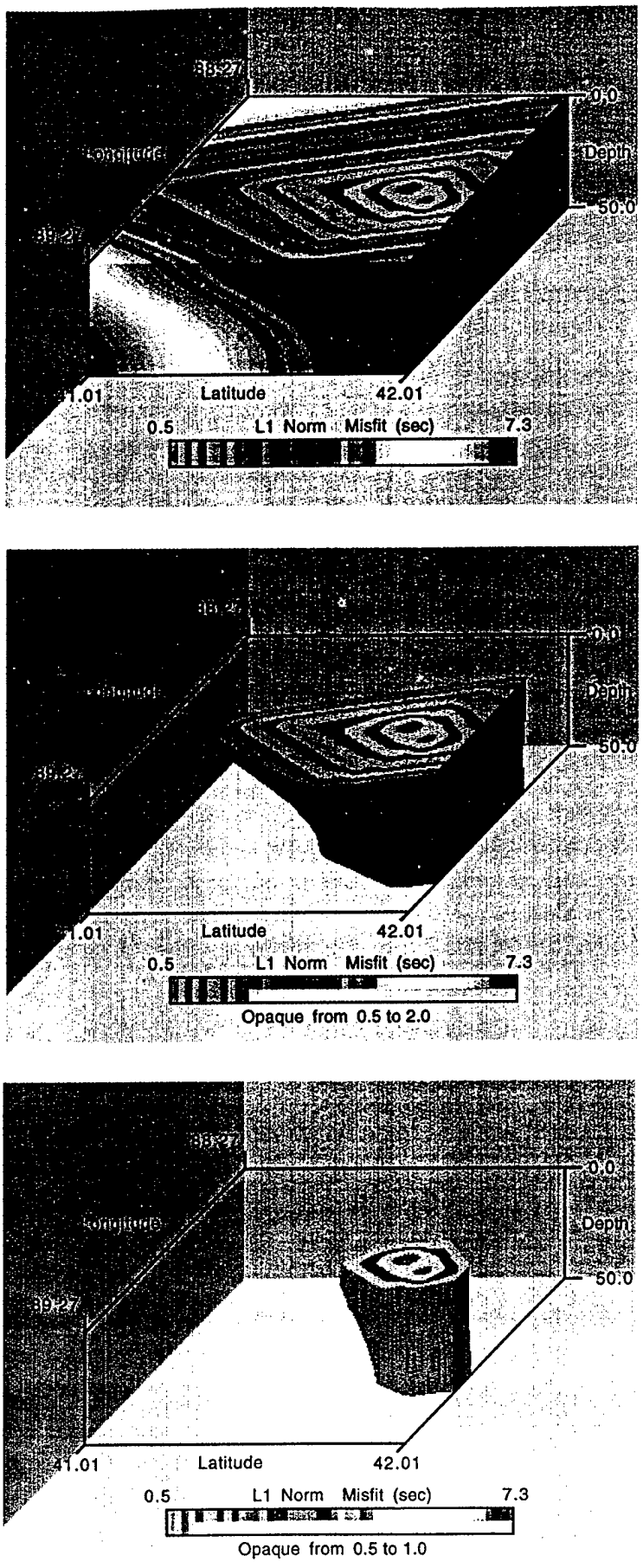

Figure 33. Four station grid search misfit volume (no SSSCs).

M98004333

Report Number (14) LA-UR--98-4876

Publ. Date (11) 199803

Sponsor Code (18) DOE/OP, XF

UC Category (19) UC-703, DOE/ER

DOE